Article

Cell Reports

LIN28B Underlies the Pathogenesis of a Subclass of Ewing Sarcoma

Graphical Abstract

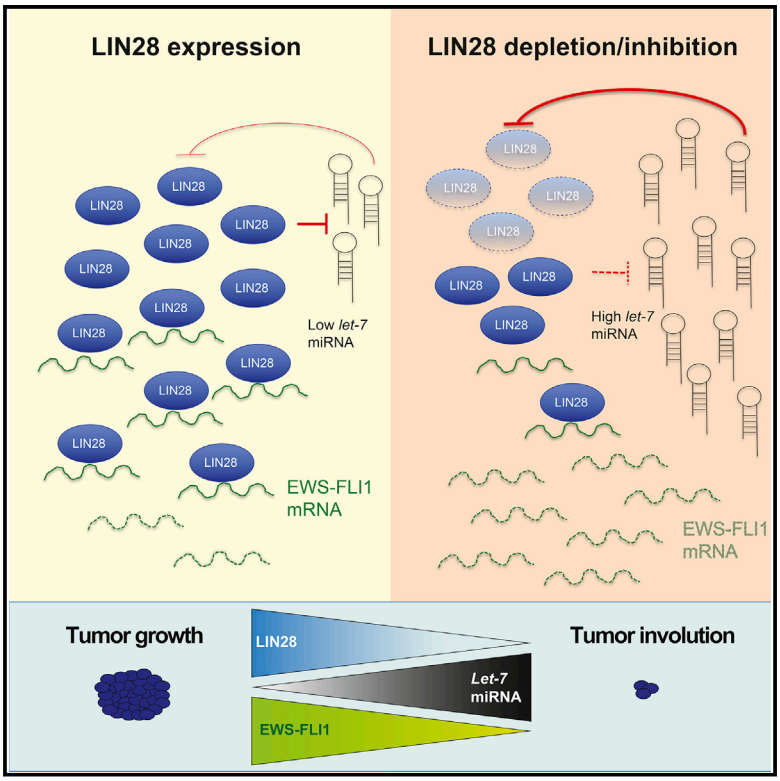

Highlights

- Lin28B expression identifies a subset of Ewing sarcomas
- Lin28B binds and stabilizes EWS-FLI-1 transcripts in these tumors
- Depletion or inhibition of Lin28B results in the deconstruction of the tumors
- Lin28B may provide a therapeutic target in a subset of Ewing sarcomas

Authors

Tugba Keskin, Arnaud Bakaric, Patricia Waszyk, ..., Miguel N. Rivera, Nicolò Riggi, Ivan Stamenkovic

Correspondence

ivan.stamenkovic@chuv.ch

In Brief

Keskin et al. show that Lin28B directly binds EWS-FLI-1 and maintains its stability in ~10% of Ewing sarcomas. Lin28B depletion or its chemical inhibition in these tumors results in the loss of EWS-FLI-1 expression and tumor deconstruction. Lin28B may provide an attractive therapeutic target in a subset of Ewing sarcomas.

Keskin et al., 2020, Cell Reports *30*, 4567–4583
March 31, 2020
https://doi.org/10.1016/j.celrep.2019.12.053

CellPress

Cell Reports
Article

LIN28B Underlies the Pathogenesis of a Subclass of Ewing Sarcoma

Tugba Keskin,[1,14] Arnaud Bakaric,[1,14] Patricia Waszyk,[1,14] Gaylor Boulay,[2,13,14] Matteo Torsello,[1,7] Sandrine Cornaz-Buros,[1,3] Nadja Chevalier,[1,10] Thibaud Geiser,[1] Patricia Martin,[1] Angela Volorio,[1,2] Sowmya Iyer,[2] Anupriya Kulkarni,[2] Igor Letovanec,[4] Stéphane Cherix,[5] Gregory M. Cote,[6] Edwin Choy,[6] Antonia Digklia,[7] Michael Montemurro,[7] Ivan Chebib,[8] Petur G. Nielsen,[8] Angel M. Carcaboso,[9] Jaume Mora,[9] Raffaele Renella,[10] Mario L. Suvà,[2] Carlo Fusco,[1] Paolo Provero,[11,12] Miguel N. Rivera,[2,13,15] Nicolò Riggi,[1,15] and Ivan Stamenkovic[1,15,16,*]
[1]Experimental Pathology Service, Centre Hospitalier Universitaire Vaudois, University of Lausanne, 1011 Lausanne, Switzerland
[2]Department of Pathology and Center for Cancer Research, Massachusetts General Hospital and Harvard Medical School, Boston, MA 02114, USA
[3]Department of Pediatrics, Centre Hospitalier Universitaire Vaudois, University of Lausanne, 1011 Lausanne, Switzerland
[4]Department of Pathology, Centre Hospitalier Universitaire Vaudois, University of Lausanne, 1011 Lausanne, Switzerland
[5]Department of Orthopaedics and Traumatology, Centre Hospitalier Universitaire Vaudois, University of Lausanne, 1011 Lausanne, Switzerland
[6]Center for Sarcoma and Connective Tissue Oncology, Massachusetts General Hospital, Boston, MA 02114, USA
[7]Department of Oncology, Centre Hospitalier Universitaire Vaudois, University of Lausanne, 1011 Lausanne, Switzerland
[8]Department of Pathology, Massachusetts General Hospital and Harvard Medical School, Boston, MA 02114, USA
[9]Department of Pediatric Hematology and Oncology, Hospital Sant Joan de Déu, 08950 Barcelona, Spain
[10]Department Woman-Mother-Child, Division of Pediatrics, Centre Hospitalier Universitaire Vaudois, University of Lausanne, 1011 Lausanne, Switzerland
[11]Center for Translational Genomics and Bioinformatics, San Raffaele Scientific Institute, 20132 Milan, Italy
[12]Department of Molecular Biotechnology and Health Sciences, University of Turin, 10124 Turin, Italy
[13]Broad Institute of Harvard and MIT, Cambridge, MA 02142, USA
[14]These authors contributed equally
[15]Senior author
[16]Lead Contact
*Correspondence: ivan.stamenkovic@chuv.ch
https://doi.org/10.1016/j.celrep.2019.12.053

SUMMARY

Ewing sarcoma (EwS) is associated with poor prognosis despite current multimodal therapy. Targeting of EWS-FLI1, the fusion protein responsible for its pathogenesis, and its principal downstream targets has not yet produced satisfactory therapeutic options, fueling the search for alternative approaches. Here, we show that the oncofetal RNA-binding protein LIN28B regulates the stability of *EWS-FLI1* mRNA in ~10% of EwSs. LIN28B depletion in these tumors leads to a decrease in the expression of EWS-FLI1 and its direct transcriptional network, abrogating EwS cell self-renewal and tumorigenicity. Moreover, pharmacological inhibition of LIN28B mimics the effect of LIN28B depletion, suggesting that LIN28B sustains the emergence of a subset of EwS in which it also serves as an effective therapeutic target.

INTRODUCTION

Ewing sarcoma (EwS) is the second most common bone malignancy in children and young adults. Its distinguishing biological feature is a unique set of reciprocal chromosomal translocations that generate fusions between *EWS* and one of several genes encoding ETS family transcription factors, the most common being *FLI1* (Riggi and Stamenkovic, 2007). The EWS-FLI1 fusion protein underlies EwS pathogenesis and behaves as an aberrant transcription factor that can induce both transcriptional activation and repression. Upon binding to GGAA repeat elements, EWS-FLI1 induces chromatin relaxation and the recruitment of chromatin-remodeling enzymes to activate *de novo* enhancers at genomic regions that are normally devoid of any regulatory function in other cell types (Boulay et al., 2017; Riggi et al., 2014; Tomazou et al., 2015). In contrast, by displacing more active wild-type ETS transcription factors from enhancers containing non-repetitive canonical ETS motifs, EWS-FLI1 causes target gene repression (Riggi et al., 2014). EWS-FLI1 therefore behaves as an oncogenic pioneer factor that can reprogram the regulatory and transcriptional features of permissive primary cells, leading to their malignant transformation.

EwS has a strong tendency toward relapse and dissemination. Recurring and metastatic disease respond poorly even to the most aggressive forms of multimodal therapy that are available and are associated with a high mortality rate (Pishas and Lessnick, 2016). Although the search for effective therapeutic strategies continues to be intense, with some potentially promising leads (Cornaz-Buros et al., 2014; De Vito et al., 2012; Engert et al., 2015; Erkizan et al., 2009; Vormoor and Curtin, 2014),

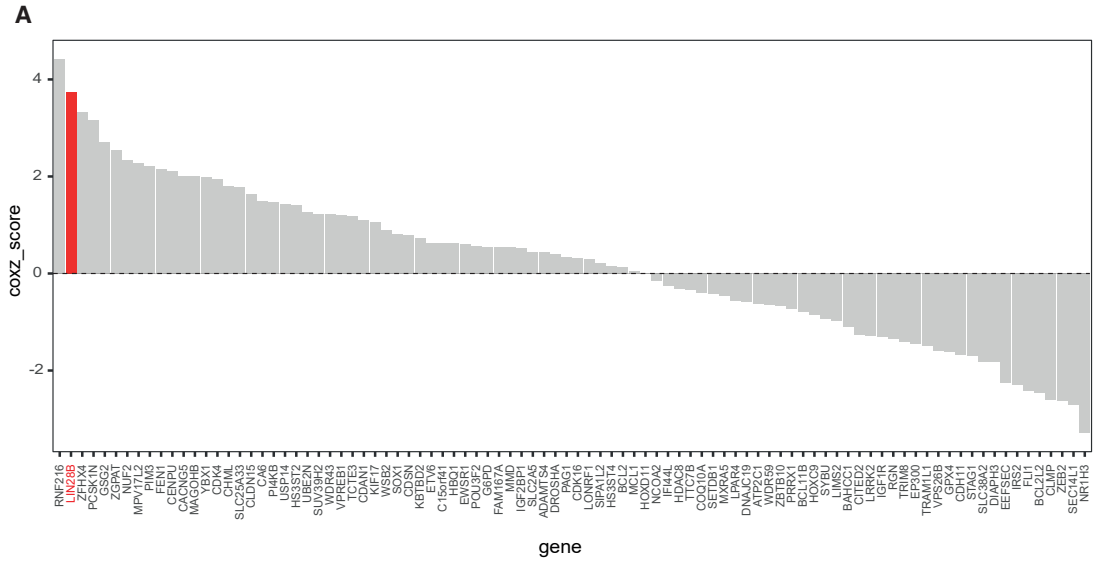

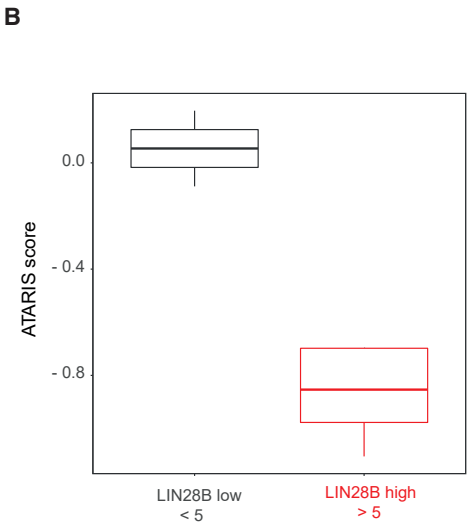

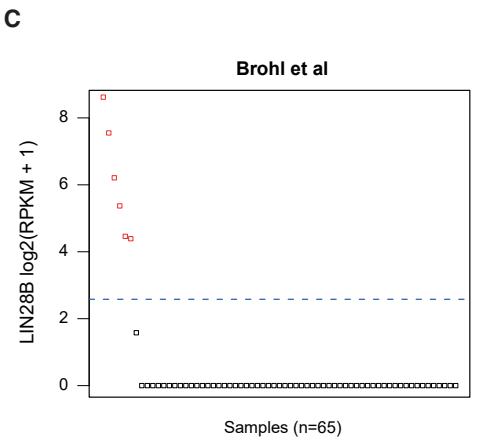

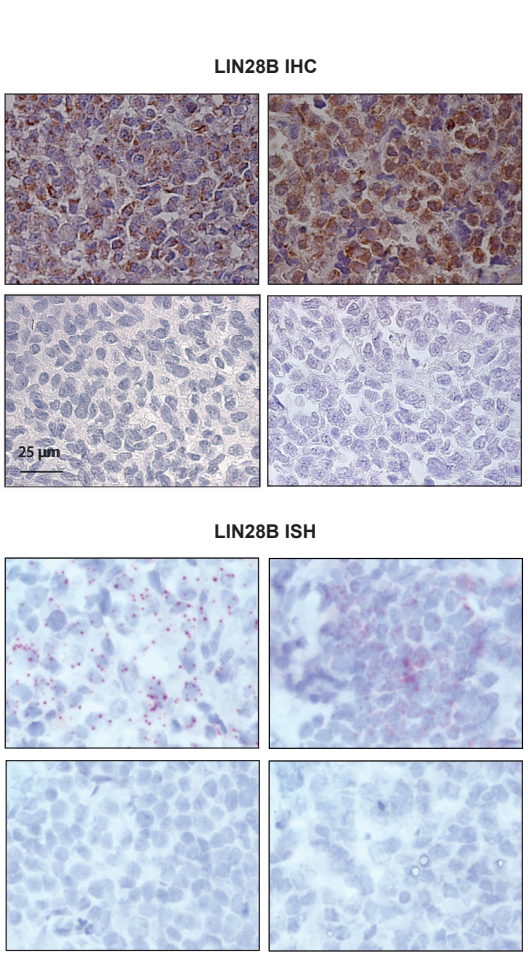

(legend on next page)

few options are available when the standard first-line combination of surgery and cytotoxic drugs fails. The unstructured features of EWS-FLI1 hinder its direct targeting (Dunker and Uversky, 2010), and therapeutically accessible regulators and downstream effectors of EWS-FLI1 that are vital to EwS growth have thus far been elusive. One relatively unexplored avenue is the search for factors that may complement or synergize with the oncogenic function of EWS-FLI1, and whose targeting may indirectly blunt EwS aggressiveness and improve patient survival. To identify such putative factors, we addressed the effects on patient survival of the top 100 genes observed to affect EwS cell growth in a recently published whole-genome CRISPR screen (Aguirre et al., 2016). Among the top candidates identified by this combinatorial approach, we found the gene that encodes the oncofetal RNA-binding protein (RBP) LIN28B.

Expression of the LIN28 paralogs (LIN28A and LIN28B) occurs during normal embryogenesis, at which time they control the balance between pluripotency and differentiation and regulate the transition from early to late embryonic development (Shinoda et al., 2013; Zhang et al., 2016). By inhibiting let-7 microRNA (miRNA) family biogenesis, LIN28A and LIN28B protect the expression of let-7 target transcripts, which include numerous pluripotency-related genes and oncogenes, thereby promoting normal stem cell maintenance and tumor growth (Madison et al., 2013, 2015; Mayr and Heinemann, 2013; Thornton and Gregory, 2012; Viswanathan and Daley, 2010). However, LIN28A and LIN28B also exert let-7-independent regulatory functions by binding to and influencing the translation of a wide repertoire of mRNAs (Balzeau et al., 2017; Viswanathan and Daley, 2010). LIN28B and, to a lesser extent, LIN28A are aberrantly expressed in a broad range of adult human malignancies associated with poor prognosis (Chatterji et al., 2018; Chatterji and Rustgi, 2018), in which they are often confined to poorly differentiated cell subpopulations that may express cancer stem cell (CSC) features (Balzeau et al., 2017; Carmel-Gross et al., 2016; Viswanathan and Daley, 2010). LIN28B is implicated in the pathogenesis of several primitive pediatric malignancies, including Wilms tumor (Urbach et al., 2014), neuroblastoma (Hennchen et al., 2015; Powers et al., 2016), and primitive neuro-ectodermal brain tumors (Choi et al., 2016; Picard et al., 2012).

Based on these observations, we addressed the potential implication of LIN28B expression in the pathogenesis of EwS. Using patient-derived EwS spheres from primary LIN28B$^+$ and LIN28B$^-$ tumors, we show that LIN28B-expressing cells not only generate tumor growth more rapidly than their LIN28B$^-$counterparts but are also dependent on LIN28B expression to sustain their self-renewal and tumor-initiating properties. We demonstrate that LIN28B directly binds *EWS-FLI1* transcripts, increasing their stability and ensuring the maintenance of EWS-FLI1 expression in tumor cells. Consequently, LIN28B depletion or pharmacological inhibition in primary EwS cells decreases the expression of both the fusion protein and its direct target genes, leading to the deconstruction of the oncogenic program and the progressive loss of tumorigenic potential *in vitro* and *in vivo*. Our observations identify an EwS subset whose dependence on LIN28B provides a unique opportunity to apply a pharmacological approach toward disrupting its otherwise undruggable oncogenic driving force.

RESULTS

LIN28B Expression Identifies a Subset of EwS

To identify candidate factors whose function may influence EwS evolution and prognosis, we correlated survival in a cohort of 44 EwS patients (Savola et al., 2011) with the expression of the top 100 genes observed to affect EwS cell growth in a recent whole-genome CRISPR library screen of 33 cancer cell lines (Aguirre et al., 2016) (Table S1). In terms of prognostic relevance, *LIN28B* ranked second only to *RNF216*, which encodes a RING finger protein involved in the regulation of the nuclear factor κB (NF-κB) pathway (Chuang and Ulevitch, 2004; Nakhaei et al., 2009), known to promote EwS cell survival (Javelaud et al., 2000) (Figure 1A). Whereas LIN28B underlies the emergence and evolution of several primitive pediatric malignancies, its role in EwS is unknown, prompting us to interrogate its putative implication in EwS pathogenesis. Patients with tumors expressing *LIN28B* (n = 3) had the poorest prognosis within the cohort, with a median survival of <2 years, whereas the evolution of patients with tumors lacking *LIN28B* was less severe and included multi-year survivors (n = 41; Figure S1A). Interrogation of the Cancer Cell Line Encyclopedia database (CCLE, Broad Institute; https://portals.broadinstitute.org/ccle) (Barretina et al., 2012) revealed that 3 of the 9 EwS cell lines used in the CRISPR-Cas9 screen (CADOES1, TC32, and MHHES1; data not shown) did not express *LIN28B* and were consequently unaffected by its targeting by gene editing (Figure 1B). These observations suggest that LIN28B plays a functional role only in a subset of EwS.

We next assessed the frequency of LIN28B$^+$ EwS in other datasets. Analysis of publicly available gene expression datasets of primary EwS revealed that in a cohort of 65 patients, 6 bore LIN28B$^+$ tumors (Figure 1C) (Brohl et al., 2014). Furthermore, 3 primary EwS were LIN28B$^+$ in a microarray dataset of 44 patients (Figure S1A), and assessment of LIN28B expression in our cohort of 40 primary EwSs using immunohistochemistry (IHC)

Figure 1. LIN28B Expression Identifies a Subclass of Aggressive EwSs

(A) The waterfall plot depicts Cox survival *Z* scores for 92 of the 100 genes that selectively affect EwS cell line growth in the Achilles database (Aguirre et al., 2016). Expression of 8 genes was not recorded in the survival dataset (Savola et al., 2011).

(B) Analytic technique for assessment of RNAi by similarity (ATARiS) score distributions for cell lines that have low (<5) and high (≥5) expression levels for *LIN28B*.

(C) Scatterplot depicting LIN28B gene expression (red squares, positive; black squares, negative) across a cohort of 65 primary EwSs (Brohl et al., 2014).

(D) Immunohistochemical (IHC, upper panels) and RNA *in situ* hybridization (ISH, lower panels) assessment of LIN28B expression in primary EwS. The selected images are representative of the 40 primary EwS samples tested (the same tumor samples are shown in the IHC and ISH panels). Expression of LIN28B was observed in 4 of the 40 tumors. The top and bottom images in each panel are LIN28B$^+$ and LIN28B$^-$, respectively.

See also Figure S1and Tables S1 and S2.

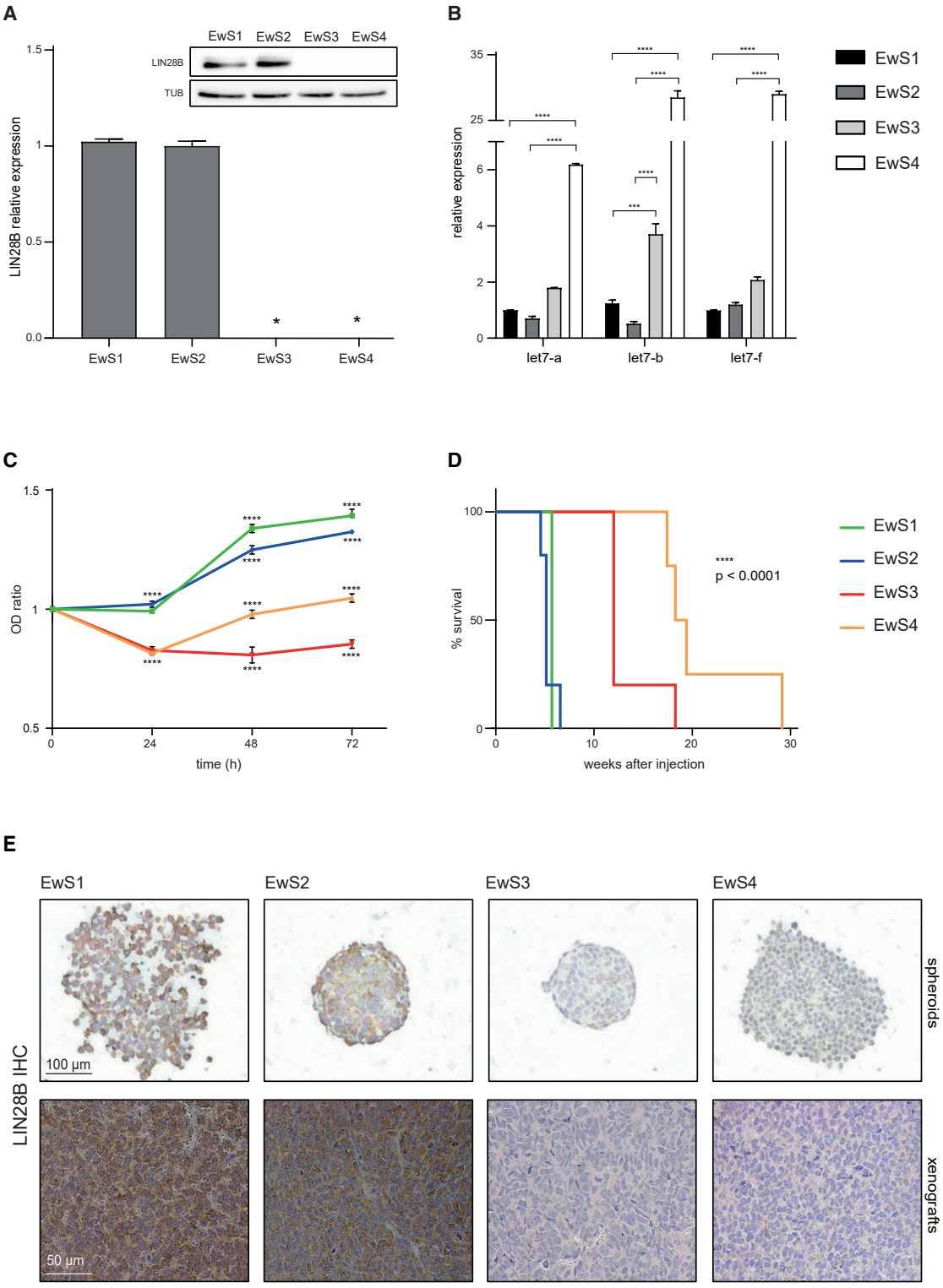

Figure 2. Primary LIN28B$^+$ and LIN28B$^-$ EwS Cells Display Different Growth Kinetics *In Vitro* and *In Vivo*

(A) qRT-PCR and western blot analyses of LIN28B expression in 4 primary EwS cell cultures (EwS1–EwS4) analyzed. Asterisks represent values that were set to 0 based on late amplification (means ± SEMs, n = 3 technical replicates).

(B) LIN28B$^+$ tumors (EwS1 and EwS2) display reduced expression levels of let-7 family members compared to their LIN28B$^-$ counterparts, as assessed by qRT-PCR analysis. Mean values ± SEMs of 3 technical replicates are shown. The statistical analysis was performed by 2-way ANOVA.

(legend continued on next page)

and *in situ* hybridization (ISH) identified 4 LIN28B$^+$ tumors (Figure 1D; data not shown). Examination of these 4 tumors revealed that LIN28B expression was uniform and not confined to cell subpopulations, as is often the case in adult malignancies. Furthermore, there was no gradation of expression among the tumors, which scored either strongly positive or negative. The sum of primary LIN28B$^+$ tumors in these 3 datasets amounted to 13 from a total of 149 (8.7%).

The recent association between *STAG2* and *TP53* mutations and poor clinical outcome in EwS patients (Brohl et al., 2014; Crompton et al., 2014; Tirode et al., 2014) prompted us to exclude a possible correlation between these mutations and *LIN28B* expression. Analysis of publicly available whole-exome and transcriptome data from primary EwS (Brohl et al., 2014) failed to reveal a statistically significant correlation between *STAG2*/*TP53* mutations and LIN28B expression (Table S2). LIN28B expression therefore appears to be a marker of a subset of EwS whose biological properties warrant assessment.

Primary LIN28B$^+$ and LIN28B$^-$ EwS Cells Have Different Growth Kinetics *In Vitro* and *In Vivo*

To address the effect of LIN28B on the behavior of EwS, we generated patient-derived spheroid cultures from 2 LIN28B$^+$ and 2 LIN28B$^-$ EwS removed at surgery (EwS1–EwS4; Table S3). The 2 primary cultures derived from LIN28B$^+$ tumors (EwS1 and EwS2) displayed robust LIN28B mRNA and protein expression, whereas neither LIN28B transcripts nor proteins were detectable in their LIN28B$^-$ tumor-derived counterparts (EwS3 and EwS4; Figure 2A). LIN28A was undetectable in any of our samples, excluding the possibility that it may substitute for its paralog in LIN28B$^-$ cells (Figure S1C). Consistent with the inhibitory effect of LIN28B on let-7 biogenesis, EwS1 and EwS2 displayed lower levels of mature let-7 than EwS3 and particularly EwS4 (Figures 2B and S1D), which bore a remarkably high expression of let-7 family members.

We then asked whether EwS cell behavior *in vitro* and *in vivo* correlates with LIN28B expression. EwS1 and EwS2 proliferated more rapidly, as assessed by MTS assays *in vitro*, with a roughly 2-fold shorter doubling time than that of EwS3 and EwS4 (Figure 2C). Following injection of 1×10^4 cells from dissociated spheres beneath the kidney capsule of NSG mice, EwS1 and EwS2 cells produced tumors after 6–8 weeks, whereas the median duration required for EwS3 and EwS4 tumor engraftment was 12 and 20 weeks, respectively (Figure 2D). EwS1 and EwS2 sphere-derived tumors maintained LIN28B expression, whereas tumors formed by EwS3 and EwS4 spheres remained LIN28B$^-$ (Figure 2E), recapitulating the original primary tumor phenotype. LIN28B expression therefore correlates with rapid EwS cell division and tumor initiation.

LIN28B Is Required for LIN28B$^+$ EwS Self-Renewal and Tumor Initiation

To determine whether LIN28B plays a role in LIN28B$^+$ EwS cell self-renewal and tumor initiation, we infected EwS1 and EwS2 cells with lentiviral vectors containing either of 2 short hairpin RNAs (shRNAs), shRNA1 and shRNA2, whose sequences target the protein coding region and the 3′ UTR of *LIN28B* mRNA, respectively. Expression of either shRNA resulted in comparable LIN28B depletion (Figure 3A, left panel, and Figure 3B) and the corresponding increase in let-7 maturation (Figure 3A, middle and right panels, and Figures S2A and S2B). LIN28B depletion virtually abolished sphere formation by EwS1 and EwS2 cells (Figure 3C). Calcein AM staining of LIN28B-depleted cells revealed a <10% decrease in viability (Figure 3D; data not shown), indicating that the observed abrogation of spherogenicity was not due to cell death. Clonogenic assays revealed a dramatic decrease in sphere formation from single EwS1 and EwS2 cells depleted of LIN28B (Figure 3E). Accordingly, 1×10^4 LIN28B-depleted EwS1 and EwS2 cells were unable to form tumors following injection beneath the kidney capsule of NSG mice (Figure 3F). Three mice injected with EwS2 cells expressing LIN28B shRNA2 developed tumors, which were found to express LIN28B at levels superior to those in control tumors (Figure S2C), having most likely originated from cells that had eluded stable LIN28B knockdown. These observations suggest that LIN28B is necessary for the maintenance of self-renewal and tumor initiation by LIN28B$^+$ EwS cells.

To exclude the possibility that the decreases in clonogenicity and tumor initiation observed using shRNAs were due to off-target effects, we attempted to rescue the LIN28B$^+$ EwS phenotype by expressing a *LIN28B* construct that lacks the 3′ UTR (*LIN28B*$^{\Delta 3UTR}$) in cells depleted of endogenous LIN28B. Following *LIN28B*$^{\Delta 3UTR}$ cDNA introduction into LIN28B$^+$ EwS cells, the endogenous transcript was depleted using shRNA2. As expected, shRNA2 affected neither transcript nor protein LIN28B levels in cells expressing exogenous *LIN28B*$^{\Delta 3UTR}$ (Figures S2D and S2E). Unlike their counterparts infected with a control vector, cells expressing *LIN28B*$^{\Delta 3UTR}$ maintained sphere formation despite the presence of shRNA2, excluding an off-target effect as an explanation for our initial observations (Figure S2F). To provide further support for our findings, we depleted *LIN28B* using CRISPR-Cas9. The expression of a validated single-guide RNA (sgRNA) sequence targeting exon 2 of *LIN28B* (Powers et al., 2016) in EwS1 cells virtually abrogated *LIN28B* mRNA and protein expression (Figures S2G and S2H) and resulted in a robust reduction in clonogenicity (Figure S2I), reproducing the phenotype obtained using shRNAs.

(C) Growth curves of the 4 spherogenic EwS cultures *in vitro* as assessed by MTS assays over 72 h. Four biological replicas were performed, and values were normalized to time point 0 (mean ± SD). Two-way ANOVA was used for statistical analysis.
(D) Survival curves of NSG mice injected with 1×10^4 EwS sphere-derived cells into the left subcapsular kidney compartment. Five mice per group were injected, and the Kaplan-Meyer test was used for statistical analysis.
(E) Immunohistochemical assessment of LIN28B expression in the 4 spherogenic EwS cultures (upper panels) and the tumors generated by their injection into NSG mice in (D) (lower panels).
***$p \leq 0.001$; ****$p \leq 0.0001$. See also Figure S1 and Table S3.

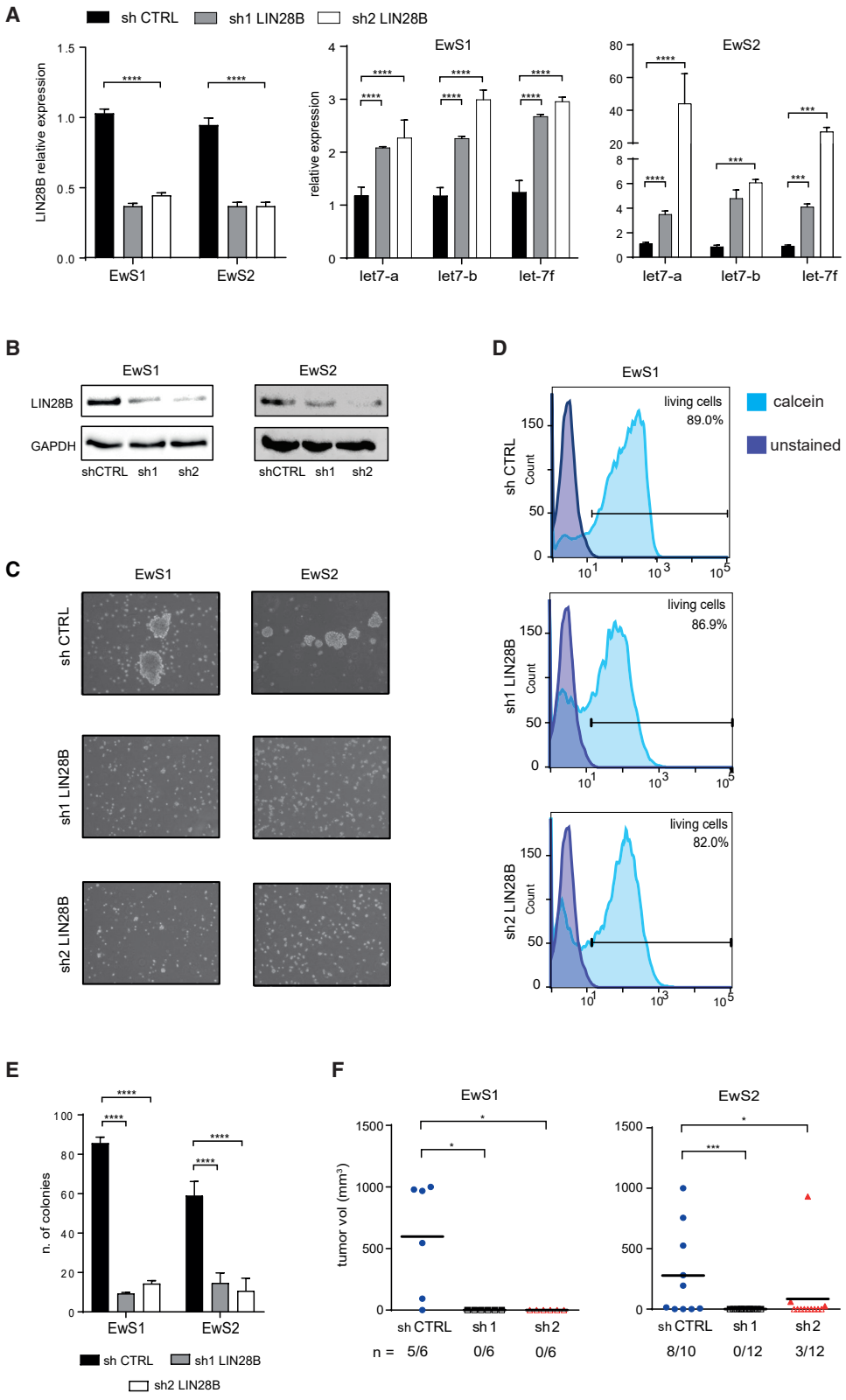

(legend on next page)

Exogenous LIN28B Expression Increases Clonogenicity of and Tumor Initiation by LIN28B^{-} EwS Spheres

We next asked whether the introduction of *LIN28B* into LIN28B^{-} tumor cells might accelerate their growth and tumor initiation by stably expressing *LIN28B*$^{\Delta\Delta 3UTR}$ in EwS3 cells (Figure 4A, left panels). As expected, LIN28B expression resulted in the suppression of let-7 family maturation and the concomitant induction of the canonical let-7 target gene *HMGA2* (Figure 4A, center and right panels, respectively). *In vitro*, EwS3 cells expressing LIN28B rapidly re-formed spheres following dissociation (Figure 4B) and displayed a 3-fold increase in clonogenicity compared to control cells (Figure 4C). Injection of LIN28B-expressing EwS3 cells under the kidney capsule of NSG mice resulted in detectable tumor growth within 8 weeks in 4 of 6 mice, reminiscent of the behavior of primary LIN28B^{+} cells (Figure 2D). The mean tumor volume at 8 weeks was ~3-fold higher than that of tumors derived from control cells (Figure 4D). Both *LIN28B* and *HMGA2* were elevated in tumors derived from LIN28B-expressing EwS3 cells (Figures 4E and 4F), compared to their empty-vector-infected counterparts. These observations support the results obtained using LIN28B-depleted cells and indicate that the expression of LIN28B alone can augment the self-renewal and tumor-forming capacity of primary EwS cells.

LIN28B Modulation Affects Expression of EWS-FLI1 and Its Target Genes

To further explore the properties of LIN28B^{+} and LIN28B^{-} EwS subtypes and interrogate the mechanism underlying LIN28B^{+} EwS cell dependence on LIN28B expression for self-renewal and tumor initiation, we compared the miRNome and transcriptome of primary LIN28B^{+} and LIN28B^{-} EwS cells using miRNA arrays and RNA sequencing (RNA-seq), respectively. EwS1 and EwS2 cells displayed a similar miRNA expression profile and the same held true for EwS3 and EwS4 cells. Although mature let-7 species were downregulated in EwS1 and EwS2 compared to EwS3 and EwS4, consistent with the inhibition of let-7 maturation by LIN28B, the corresponding miRNA target genes were not significantly overrepresented among the genes that were differentially expressed between LIN28B^{+} and LIN28B^{-} tumors (Figure 5A). Specifically, only 7 predicted let-7 targets were upregulated in LIN28B^{+} tumors (7.757 expected by chance, rendering the enrichment p value non-significant), suggesting that the LIN28B^{+} EwS phenotype may arise not only from the inhibition of let-7 biogenesis but also from the effects that LIN28B may exert on its direct target transcripts.

LIN28B affects diverse biological processes, including cell metabolism and proliferation, independent of its let-7-regulatory function (Balzeau et al., 2017). To gain deeper insight into the biological effects of LIN28B in EwS, we generated RNA-seq expression profiles of EwS1 and EwS2 cells depleted of LIN28B using shRNA2, and performed functional gene set enrichment analysis (GSEA) pathway analysis. We found a marked overlap between the list of downregulated genes in LIN28B-depleted cells and multiple gene sets related to the transcriptional function of EWS-FLI1 in EwS (Figure 5B, upper left panel, and Figure S3A). The top-scoring gene set identified by this approach was *Riggi_Ewing_Sarcoma_Progenitor_Up*, which contains the list of genes induced by EWS-FLI1 in human pediatric mesenchymal stem cells (hpMSCs) (Riggi et al., 2010). Direct comparison of this gene set to the genes repressed by LIN28B depletion revealed a highly significant overlap in both primary cell cultures (EwS1 $p = 4.8 \times 10^{-16}$, EwS2 $p = 3.4 \times 10^{-37}$; Figure 5B, lower left panel). A set of 32 genes found to be common to the 2 primary cell cultures and the GSEA gene set included numerous known EWS-FLI1 targets (Figure 5B, right panel), suggesting that LIN28B may regulate EWS-FLI1 target gene expression or, more likely, the expression and function of EWS-FLI1 itself.

To address the latter possibility, we depleted EwS1 and EwS2 cells of EWS-FLI1 using a validated shRNA sequence (De Vito et al., 2011) and conducted RNA-seq analysis on these cells and their corresponding control counterparts infected with an shRNA sequence targeting *GFP* mRNA. Comparison of RNA-seq data from EwS1and EwS2 cells depleted of either LIN28B or EWS-FLI1 revealed a striking overlap between the two expression datasets (p value for common downregulated genes $p = 8.6 \times 10^{-68}$ and 1.4×10^{-183} for EwS1 and EwS2, respectively; Figures 5C and S3B). We then compared the RNA-seq profiles of LIN28B-depleted EwS1 and EwS2 cells with a curated list of 111 EWS-FLI1-activated genes identified by combining the changes in gene expression observed upon EWS-FLI1 knock down in 2 EwS cell lines (A673 and SK-N-MC) and upon the lentiviral introduction of exogenous EWS-FLI1 into hpMSCs (Table S4) (Boulay et al., 2018). Of the 111 genes, only 99 were expressed in our RNA-seq samples and were used in the comparative analysis. Once again, we found a highly significant overlap for upregulated genes between these datasets from both

Figure 3. LIN28B Is Essential for Self-Renewal and Tumorigenic Properties of LIN28B^{+} EwS Cells

(A) qRT-PCR assessment of *LIN28B* transcript (left panel) and mature let-7 (center panel and right panels) levels in EwS1 and EwS2 cells transduced with *LIN28B*-targeting shRNAs (sh1 LIN28B and sh2 LIN28B) compared to those in the same cells transduced with GFP-targeting shRNA controls (sh CTRL). Mean values ± SEMs of 3 independent experiments are shown. Two-way ANOVA was used for statistical analysis.

(B) Western blot analysis of LIN28B protein levels in EwS1 and EwS2 cells upon shRNA-mediated LIN28B depletion in (A).

(C) Micrographs of EwS1 and EwS2 spherogenic cultures 96 h after lentiviral infection with either control or *LIN28B*-targeting shRNAs.

(D) Fluorescence-activated cell sorting (FACS) analysis of EwS1 sphere viability 96 h post-transduction with either control or *LIN28B*-targeting shRNA vectors.

(E) Clonogenic assay of EwS1 and EwS2 cultures depleted or not depleted of LIN28B (means ± SDs, n = 3 technical replicates). Two-way ANOVA was used for statistical analysis.

(F) *In vivo* tumorigenicity assay after the injection of 1×10^4 control or LIN28B-depleted EwS1 and EwS2 cells. The loss of LIN28B expression results in virtually complete abrogation of the tumorigenic potential of EwS1 and EwS2 cells. The bar indicates the mean tumor volume and n indicates the number of mice that developed tumors out of the total number of mice used in each experiment. Fisher's exact test was used for the statistical analysis of tumor counts only. Full symbols indicate visible tumors; empty symbols indicate undetectable tumor growth.

*$p > 0.05$; ***$p \leq 0.001$; ****$p \leq 0.0001$. See also Figure S2.

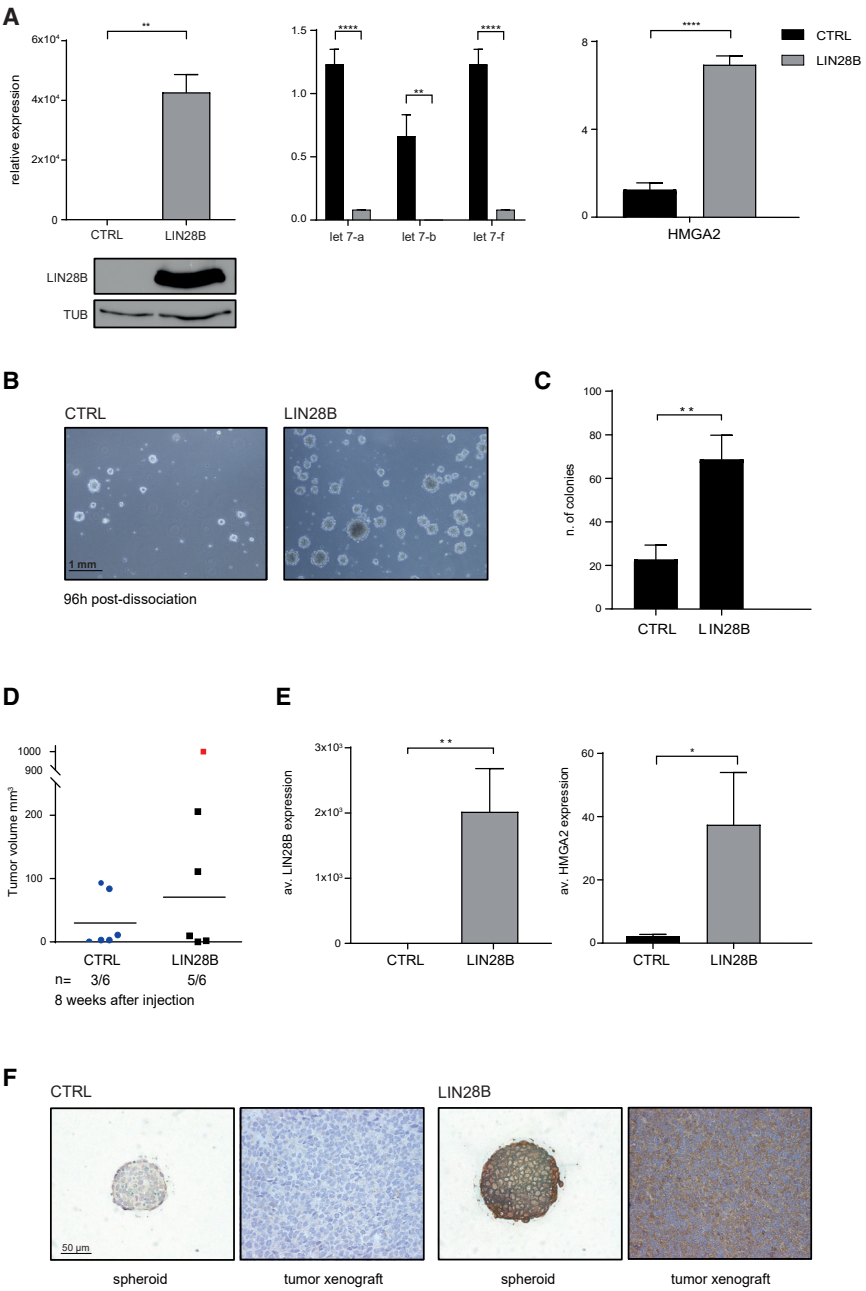

Figure 4. LIN28B Expression Increases LIN28B⁻ EwS Cell Self-Renewal and Tumorigenicity

(A) Left panel: qRT-PCR (top) and western blot (bottom) analyses of LIN28B expression in EwS3 spheres transduced with an LIN28B-expressing vector (LIN28B), compared to spheres transduced with an empty (CTRL) vector. Mean values ± SEMs of 3 independent experiments are shown. Center and right panels: qRT-PCR assessment of mature let-7a, b, and f (center) and HMGA2 (right) transcript levels in LIN28B-expressing EwS3 spheres compared to their empty-vector-infected counterparts. The means ± SEMs of 3 independent experiments are shown.

(B) Micrographs of EwS3 cultures 96 h after dissociation, showing a marked increase in the spherogenic ability of cells transduced with LIN28B.

(C) Clonogenic assays of LIN28B-expressing EwS3 cells compared to their empty-vector-infected counterparts (CTRL, means ± SDs).

(D) Injection of 1×10^4 EwS3 cells into NSG mice reveals increased tumor initiation by EwS3 cells expressing exogenous LIN28B. The letter "n" indicates the number of mice that developed tumors out of the total number of mice used in each experiment. The bar indicates the mean tumor volume. The outlier (red square) was not included in the calculation of the mean.

(E) Average *LIN28B* (left) and *HMGA2* (right) transcript levels in tumors from LIN28B-expressing EwS3 cells, as assessed by qRT-PCR (means ± SDs, n = 3 technical replicates).

(F) Immunohistochemical analysis of LIN28B protein expression in control and LIN28B-expressing EwS3 spheroids, as well as in the tumor xenografts derived from injection of the corresponding cell populations into NSG mice. Student's t test was used to perform statistical analyses in (A) and (C) (right panel) and (E) and (G); 2-way ANOVA for analysis in (C) (left panel).

*p < 0.05; **p < 0.001; ***p ≤ 0.001; ****p ≤ 0.0001.

primary EwS cell cultures ($p = 4.86 \times 10^{-26}$ and 6.8×10^{-51} for EwS1 and EwS2, respectively; Figures 5C and S3B). The same held true when the analysis was repeated for downregulated genes (Figure S3C). These data strongly support a direct functional relation between LIN28B and EWS-FLI1.

To determine the nature of this putative functional relation, we assessed possible changes in EWS-FLI1 expression upon LIN28B depletion in our two primary cell cultures. In both EwS1 and EwS2 cells, the depletion of LIN28B resulted in a robust decrease in EWS-FLI1 transcript and protein levels (Figures 5D and S3D). The effect on wild-type (WT) *EWS* was also significant in EwS1 cells, albeit slightly less marked, whereas it was not significant in EwS2 cells (Figure S3D). In contrast, *LIN28B* expression increased upon *EWS-FLI1* knockdown (Figure S3E), excluding a reciprocal positive feedback loop between the two genes. A comparable decrease in the expression of a panel of direct EWS-FLI1 target genes in response to the depletion of either *LIN28B* or *EWS-FLI1* (Figure 5E, left and center panels) further validated these results. Similar observations were made upon the depletion of *LIN28B* from EwS1 cells using CRISPR-Cas9 (Figure 5E, right panel).

LIN28B Stabilizes EWS-FLI1 Transcripts

To address the possibility that LIN28B may protect *EWS-FLI1* transcripts from let-7-mediated silencing, we attempted to overexpress let-7a in EwS1 and EwS2 spheres. However, we were

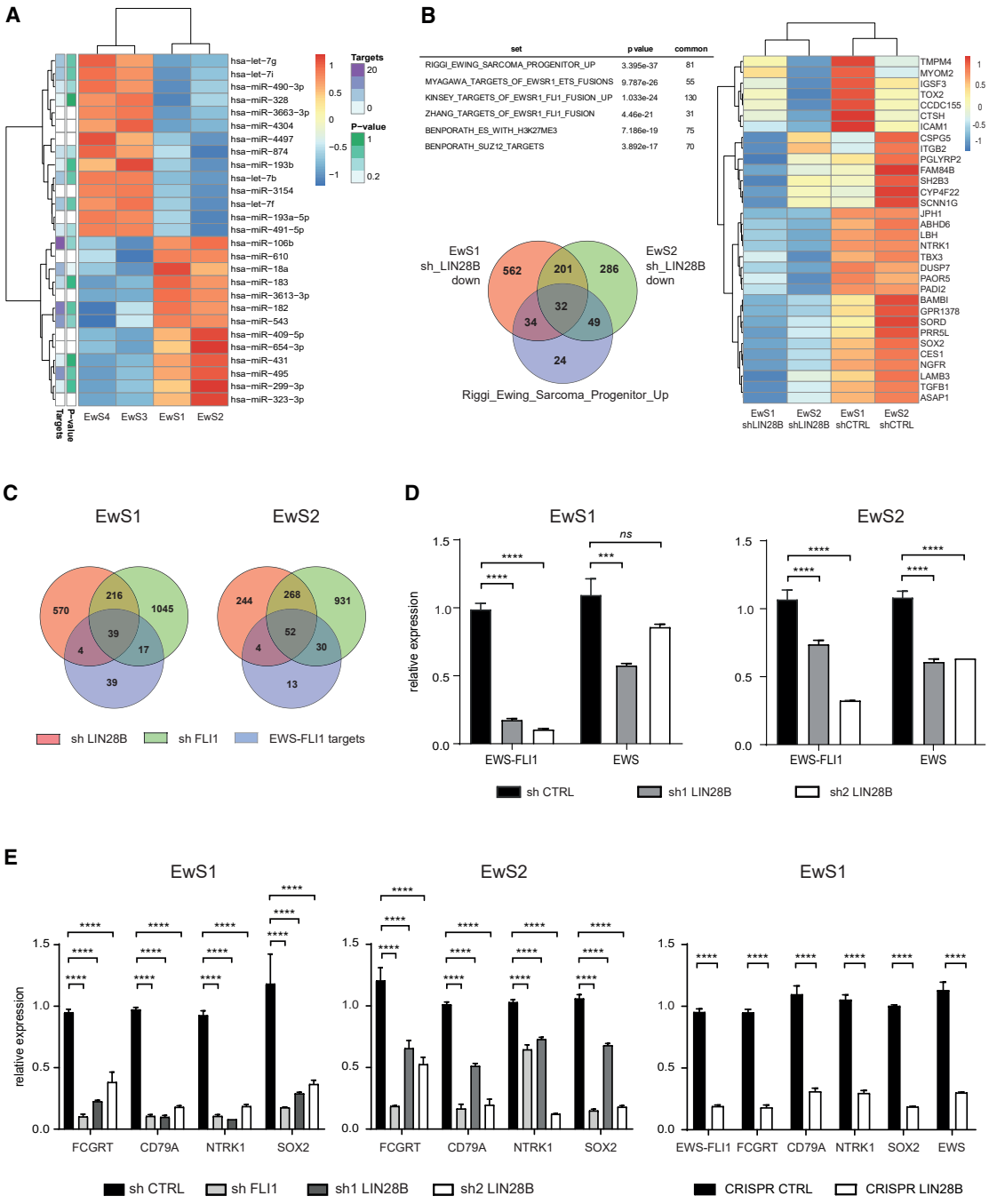

Figure 5. LIN28B Regulates EWS-FLI1 Expression in LIN28B$^+$ EwS Cells

(A) Heatmap of *Z* scores of differentially expressed miRNAs between LIN28B$^+$ and LIN28B$^-$ EwS cells. The number of discordant predicted targets (down-regulated in response to upregulated miRNAs and vice versa) and the corresponding enrichment p values are shown at left. White cells correspond to poorly conserved miRNA families for which no high-confidence target predictions are available in TargetScan.

(B) Top panel: functional GSEA pathway analysis of EwS2 cells depleted of LIN28B using shRNA2. Bottom panel: Venn diagram depicting the overlap among genes repressed by LIN28B depletion in EwS1 and EwS2 cells and the "*Riggi_Ewing_Sarcoma_Progenitor_Up*" GSEA gene set (bottom). Right panel: gene expression heatmap of the 32 shared genes in the Venn diagram.

(C) Venn diagrams illustrating the overlap between genes repressed by *LIN28B* and *EWS-FLI1* depletion in EwS1 and EwS2 cells, as well as part of a curated list of 99 direct EWS-FLI1 target transcripts.

(D) qRT-PCR assessment of *EWS-FLI1* and WT *EWS* expression in EwS1 and EwS2 cells following shRNA-mediated *LIN28B* depletion. Means ± SEMs of 3 independent experiments are shown.

(legend continued on next page)

unable to obtain overexpression, most likely because of let-7 toxicity in EwS cells (De Vito et al., 2011). We therefore interrogated the TargetScanHuman 7.1 web tool (Agarwal et al., 2015), but found that *EWS-FLI1* mRNA does not contain any let-7 binding sites. A reasonable assumption then may be that as an RBP targeting a broad repertoire of mRNAs, LIN28B binds *EWS-FLI1* transcripts and preserves their expression. Consistent with this hypothesis, *EWS-FLI1* was enriched in LIN28B RNA immunoprecipitation (RIP) assays on the lysates of both EwS1 and EwS2 cells (Figure 6A). WT *EWS* transcripts were also enriched in LIN28B RIPs (Figure 6A), whereas *FLI1* mRNA is not expressed in EwS cells. To distinguish between the possible effects of LIN28B on *EWS-FLI1* transcription versus stability, we assessed EWS-FLI1 and its target gene nascent mRNA levels in the presence and absence of LIN28B. Whereas nascent *EWS-FLI1* transcripts were unaffected by LIN28B depletion, all of its selected target gene transcript levels displayed a marked decrease (Figure 6B), refuting LIN28B-mediated control of *EWS-FLI1* transcription and pointing toward the regulation of its stability. To further examine this potential mechanism of action, actinomycin D (ActD)-mediated blockade of transcription was conducted in EwS2 cells in the presence and absence of LIN28B, and *EWS-FLI1* transcript levels were measured by qRT-PCR. Depletion of LIN28B led to the observed decrease in *EWS-FLI1* transcripts, and treatment with ActD resulted in a significant, additional decrease in *EWS-FLI1* expression (Figure 6C, upper panel). To obtain deeper insight into the effect of LIN28B on *EWS-FLI1* stability, we addressed changes in *EWS-FLI1* expression at early time points following ActD administration in the presence or absence of LIN28B. ActD alone revealed that the half-life of *EWS-FLI1* was 5.9 and 5.2 h in EwS1 and EwS2 cells, respectively (Figures 6C and S3F). In the absence of LIN28B, the *EWS-FLI1* transcript half-life was reduced to 2 h in both primary cultures (Figures 6C and S3F). In the LIN28B$^-$ EwS3 cells, the half-life of *EWS-FLI1* was 1.7 h, comparable to that in EwS1 and EwS2 cells depleted of LIN28B (Figure S3G). These observations support the notion that by directly binding *EWS-FLI1* transcripts, LIN28B protects them from degradation. Accordingly, the depletion of either LIN28B or EWS-FLI1 in EwS1 and EwS2 cells produced a comparable decrease in their proliferation (Figure S3H).

The demonstration that LIN28B stabilizes *EWS-FLI1* mRNAs suggests that it may boost EWS-FLI1 expression. However, the expression of EWS-FLI1 and that of its direct target genes was not higher in LIN28B$^+$ than in LIN28B$^-$ EwS cells (Figure S4A), nor did the expression of EWS-FLI1 increase in EwS3 cells (LIN28B$^-$) upon the introduction of *LIN28B*$^{\Delta 3UTR}$ (Figure S4B). Furthermore, comparison of differentially expressed genes in EwS1 and EwS2 cells depleted of LIN28B to those in EwS3 cells overexpressing LIN28B revealed no significant overlap (Figure S4C), indicating that exogenous LIN28B expression in LIN28B$^-$ EwS cells does not recreate the naturally occurring LIN28B$^+$ EwS phenotype.

LIN28B$^-$ EwS cells may have developed different mechanisms to ensure EWS-FLI1 stability, rendering LIN28B redundant. Full assessment of the effect of LIN28B may therefore require a cellular environment that is permissive for EWS-FLI1 expression and function but that does not naturally express the fusion protein. To test this possibility, we engineered primary hpMSCs to conditionally express EWS-FLI1 cDNA under the control of a doxycycline-inducible promoter and infected them with lentiviruses containing *LIN28B* or an empty control vector. Expression of EWS-FLI1 was then induced by treating the cells with doxycycline and the expression level of EWS-FLI1, as well as that of a panel of its target genes in LIN28B-expressing and LIN28B$^-$ hpMSCs, were compared. Using 2 unrelated primary hpMSC batches, we observed ~3-fold higher *EWS-FLI1* expression in cells expressing LIN28B and an even greater difference in its expression at the protein level (Figures 6D and S4D). The augmented EWS-FLI1 expression in LIN28B-expressing hpMSCs was accompanied by a corresponding increase in the expression of a selection of its target genes, including *AMER2*, *SOX2*, *CCK*, *NKX2.2*, and *NGFR* (Figures 6D and S4D), ranging from slightly less than 1.5-fold for *NKX2.2* to >10-fold for *CCK*. These observations support the LIN28B-mediated stabilization of *EWS-FLI1* transcripts in the appropriate cellular environment. They also confirm that the mechanism of *EWS-FLI1* maintenance by LIN28B is let-7 independent, since the *EWS-FLI1* expression construct used in hpMSCs lacks the 3′ UTR. These observations point to a hitherto unrecognized regulatory mechanism of *EWS-FLI1* expression that is exploited by a subclass of EwS.

Treatment with LIN28 Inhibitor 1632 Impairs *In Vitro* Clonogenicity and *In Vivo* Growth of LIN28B$^+$ but Not LIN28B$^-$ EwS Cells

The observation that LIN28B stabilizes *EWS-FLI1* expression renders its inhibition a potentially attractive means to treat the subset of tumors that express LIN28B. Recently, the small molecule 1632 (*N*-methyl-N-[3-(3-methyl[1,2,4]triazolo[4,3-*b*]-pyridazin-6-yl)phenyl]acetamide) was shown to block the recognition of let-7 miRNA precursors by the LIN28 paralogs (Roos et al., 2016). Because the let-7 miRNA family directly regulates LIN28 expression, we reasoned that the 1632 inhibitor may provide a pharmacological means to disrupt EWS-FLI1 expression in LIN28B$^+$ EwS, by the repression of LIN28B itself. Treatment with the 1632 inhibitor at 2 different concentrations (50 and 250 μM) for different durations (4–7 days) elicited different responses in LIN28B$^+$ and LIN28B$^-$ EwS cells. In EwS1 and EwS2 cells, the compound caused a robust increase in let-7 maturation (Figure 7A, left panel, and Figure S5A; data not shown) and a corresponding decrease in the expression of the LIN28B target gene *HMGA2* (Figure 7A, right panel). In contrast, the expression of immature and mature let-7 forms did not undergo a significant change in EwS3 and EwS4 cells in response to the inhibitor (Figure 7A, left panel; data not shown), and *HMGA2* expression displayed no significant decrease in either

(E) Expression of a panel of known direct EWS-FLI1 target genes in EwS1 and EwS2 cells following shRNA- (left and center panels) and CRISPR-Cas9-mediated (right panel) *LIN28B* depletion. shRNA- and CRISPR-Cas9-LIN28B-depleted cells were compared to *GFP*-targeting shRNA and CRISPR-Cas9 control guide RNA vector-infected cells, respectively. Means ± SEMs of 3 independent experiments are shown. Two-way ANOVA was used for statistical analysis.
***$p \leq 0.001$; ****$p \leq 0.0001$; ns, non-significant. See also Figures S3 and S4 and Table S4.

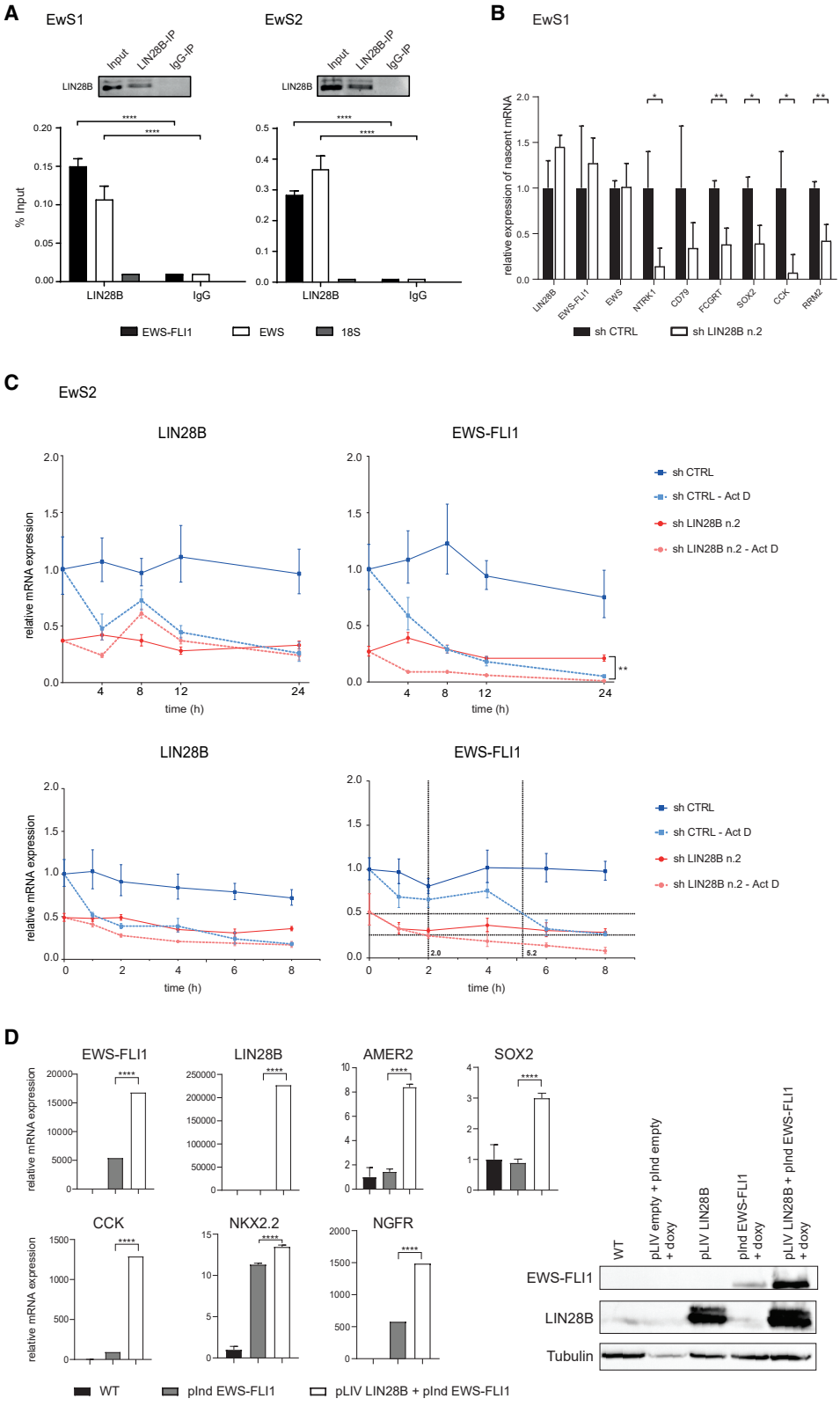

(legend on next page)

primary cell culture (Figure 7A, right panel). Consistent with these observations, functional assays revealed that after 96 h of treatment with the inhibitor at 250 μM, EwS1 and EwS2 cells lost their ability to re-form spheres following dissociation, whereas sphere formation by EwS3 and EwS4 remained unaffected irrespective of the concentration of the compound or treatment duration (Figures 7B and S5B, upper panel; data not shown). Consistent with our observations on the effect of LIN28B depletion, survival of the 4 primary cultures was not significantly affected by the compound (Figure S5B, lower panel). Clonogenic assays using all 4 primary cell cultures pre-treated with the inhibitor for 96 h and then treated continuously at 250 μM for 2 weeks showed an unequivocal decrease in sphere-forming capacity by single EwS1 and EwS2 cells, but no change in EwS3 and EwS4 cell clonogenicity (Figure 7C).

We next sought to determine whether the treatment of LIN28B$^+$ cells with the 1632 inhibitor results in the expected decrease in EWS-FLI1 expression, as initially hypothesized. In response to the compound at 250 μM, both EWS and EWS-FLI1 protein expression was abolished in EwS1 cells (Figure S5C). We then performed an RNA-seq analysis on EwS1 spheres that had been cultured in the presence of the inhibitor for 7 days and compared the resulting gene expression profile with the ones obtained following LIN28B and EWS-FLI1 depletion. Once again, we observed a statistically significant overlap between the expression profile of 1632-treated EwS1 cells and the different datasets ($p = 1.32 \times 10^{-34}$, 3.77×10^{-51}, and 4.92×10^{-23} for shLIN28B, shEWS-FLI1, and EWS-FLI1 target genes, respectively; Figures 7D and S5D). These results were validated by the assessment of changes in the expression of LIN28B, EWS-FLI1, and EWS-FLI1 target genes in EwS1 cells treated with the 1632 inhibitor for 7 days (Figure 7E).

As the 1632 compound has not been tested *in vivo*, we could not assess the effect of its continuous infusion on tumors growing in mice. Nevertheless, to determine whether the observed effect on clonogenicity is reflected by the inhibition of tumor growth *in vivo*, we injected 1×10^4 EwS1 and EwS2 cells under the kidney capsule of NSG mice after 96 h of pre-treatment with 250 μM of the 1632 inhibitor or DMSO. All of the mice were sacrificed 8 weeks post-injection, when tumors in untreated mice had grown to the maximal size allowed by the animal experimentation ethics commission. Despite the suboptimal treatment conditions, we observed a robust decrease in the size of tumors derived from treated EwS1 and EwS2 cells (Figure 7F). These observations demonstrate the feasibility of suppressing EWS-FLI1 and its oncogenic effects by targeting the LIN28B-dependent mechanism that maintains its expression.

DISCUSSION

Using an unbiased approach to search for factors that associate with EWS-FLI1 in promoting EwS pathogenesis, we identified LIN28B as a regulator of EWS-FLI1 expression and function in a small percentage of EwSs that depend on LIN28B for the expression and maintenance of their identity. A possible outcome of this discovery is that EwSs expressing LIN28B may be sensitive to its inhibition, warranting further investigation of LIN28B as a therapeutic target in some cases of EwS.

The RBPs LIN28A and LIN28B abrogate the processing of primary and precursor let-7 family hairpins into mature let-7 miRNAs (Mayr and Heinemann, 2013; Thornton and Gregory, 2012; Viswanathan and Daley, 2010) and help maintain normal development and pluripotency by preventing let-7-induced differentiation in mouse embryonic stem cells (Zhang et al., 2016). Conversely, mature let-7 represses LIN28B translation as part of a negative feedback loop (Thornton and Gregory, 2012; Zhang et al., 2016). The maintenance of pluripotency and the protection of numerous oncogenes from let-7-mediated silencing are thought to be the principal mechanisms by which LIN28B promotes cancer growth and progression. However, as our observations suggest, LIN28B may also exert oncogenic properties by directly binding to mRNA (Mayr and Heinemann, 2013), which is consistent with the notion that the most abundant class of RNAs bound by LIN28B is protein coding transcripts (Hafner et al., 2013). A recently identified LIN28B target mRNA was *TLS/FUS,* a close relative of *EWS*, which, similar to *EWS*, partners with several genes to generate oncogenic fusion proteins (Wilbert et al., 2012).

The introduction of LIN28B into LIN28B$^-$ primary EwS cells conferred increased proliferation and clonogenicity, as well as accelerated tumor-initiating capacity onto the cells, all of which are consistent with the effects that LIN28B exerts on diverse tumor cell types (Viswanathan et al., 2009). The mechanisms underlying these effects are most likely a combination of let-7 maturation suppression and modulation of the stability of the

Figure 6. LIN28B Controls *EWS-FLI1* Transcript Stability in LIN28B$^+$ EwS Cells

(A) RNA immunoprecipitation assay (RIP). qRT-PCR analysis of *EWS-FLI1* and WT *EWS* transcripts in EwS1 and EwS2 cells following LIN28B protein immunoprecipitation (upper panel). The *18S* gene was used as an internal control, and results were compared to non-specific isotype-matched immunoglobulin G (IgG) immunoprecipitates. Student's t test was used for statistical analysis.

(B) Nascent RNA assay for *EWS-FLI1* and EWS-FLI1 target transcripts in the presence and absence of LIN28B in EwS1 cells. LIN28B-targeting shRNA has no effect on nascent *EWS-FLI1* mRNA, whereas it strongly depletes EWS-FLI1 target transcripts (means ± SDs of 3 technical replicates).

(C) Analysis of transcript levels upon ActD treatment, suggesting that LIN28B regulates *EWS-FLI1* RNA stability in EwS2 cells. EwS2 cells were subjected to LIN28B depletion for 36 h, after which 10 μM ActD or solvent (equivalent volume of DMSO) was added for an additional 24 h, during which *LIN28B* and *EWS-FLI1* expression was measured (upper panel). To determine the half-life of *EWS-FLI1*, the decay rate was measured by qRT-PCR at 5 time points over 8 h in the presence of ActD (lower panel). *EWS-FLI1* transcript half-life, as estimated from the expression curves, is indicated.

(D) Left panel: expression of EWS-FLI1, LIN28B, and a panel of known direct EWS-FLI1 target genes in hpMSC1, infected with pInd EWS-FLI1 or co-infected with pInd EWS-FLI1 and pLIV LIN28B, respectively (mean values ± SDs of 3 technical replicates). EWS-FLI1 was induced by doxycycline treatment for 8 days. Student's t test was used for statistical analysis. Right panel: western Blot analysis of EWS-FLI1 and LIN28B expression in hpMSC1 infected with the indicated lentiviral vectors and cultured with (+ doxy) or without doxycycline for 8 days.

*$p \leq 0.05$, **$p \leq 0.01$; ****$p \leq 0.0001$. See also Figures S3 and S4.

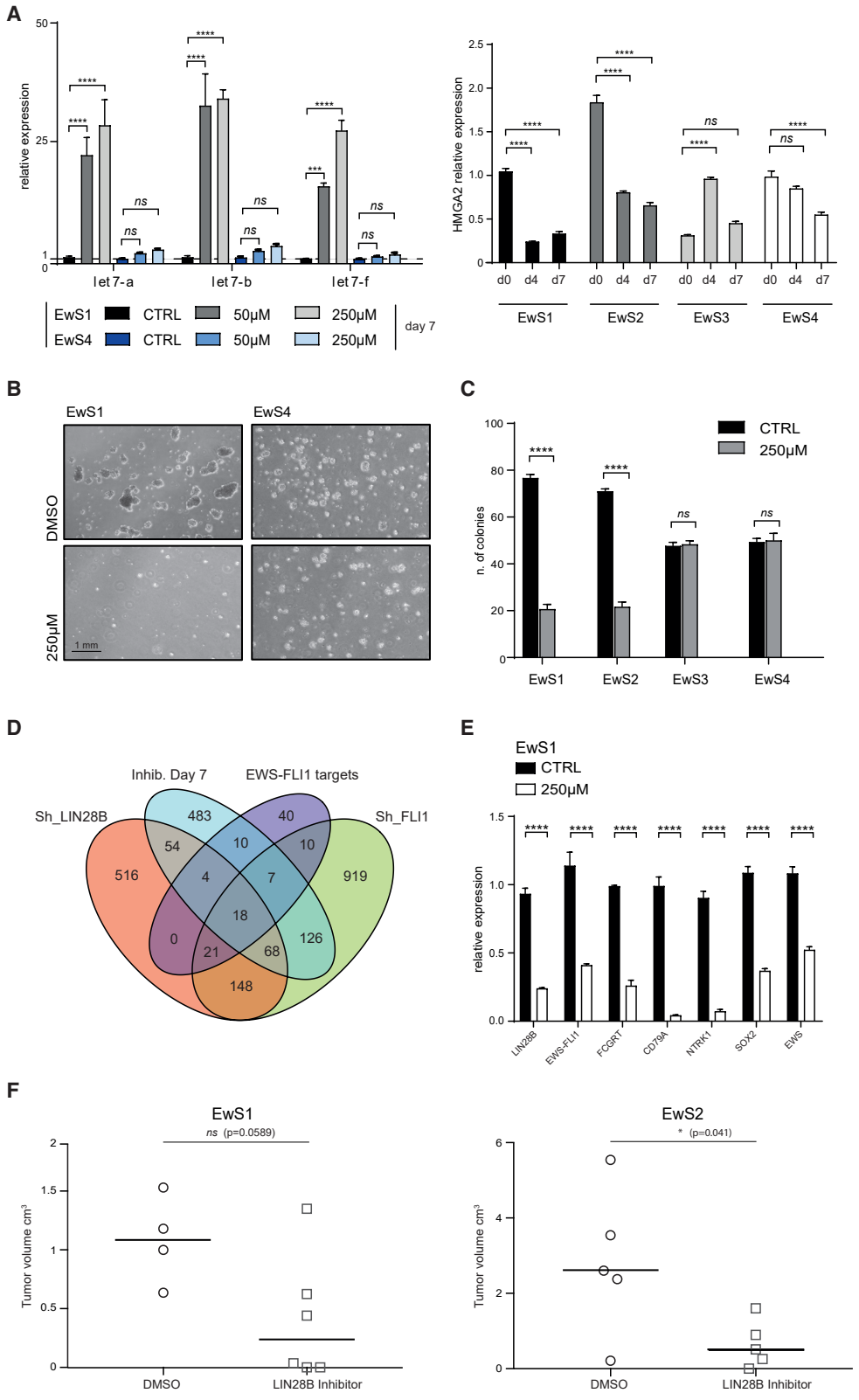

(legend on next page)

available repertoire of direct LIN28B target transcripts. However, exogenous LIN28B affected neither EWS-FLI1 expression nor that of its target gene repertoire in EwS cells. Thus, the changes in the behavior of these cells in response to the introduction of LIN28B were not the result of altered EWS-FLI1 expression or function but rather the superposition of the respective oncogenic properties of LIN28B and EWS-FLI1.

In stark contrast was the effect of depleting LIN28B$^+$ EwS cells of their endogenous LIN28B, which included a dramatic decrease in EWS-FLI1 expression along with that of its direct target genes, accompanied by the loss of self-renewal and tumor initiation. By far the most dominant trait of the transcriptome change associated with LIN28B depletion was the suppression of direct EWS-FLI1 target transcripts. Changes related to let-7 maturation and binding of LIN28B to other mRNA targets were not comparable to those of the EWS-FLI1 target gene repertoire. From a functional standpoint, depletion of EWS-FLI1 or LIN28B alone from these cells decreased their proliferation to a similar degree, despite the fact that LIN28B transcripts increased more than 2-fold in response to EWS-FLI1 knockdown. LIN28B therefore appears to provide indispensable support for EWS-FLI1 expression and function in these cells, and the absence of let-7 recognition sites in *EWS-FLI1* argues that LIN28B itself bears responsibility for the stability of *EWS-FLI1*.

The depletion of LIN28B in LIN28B$^+$ EwS cells resulted in a decrease in *EWS-FLI1* transcript half-life to a level in the vicinity of that observed in LIN28B$^-$ cells. As EWS-FLI1 expression in LIN28B$^-$ cells is sufficient to allow it to fulfill its oncogenic functions, these cells must either possess an alternative mechanism to ensure *EWS-FLI1* stability or lack the putative machinery that degrades *EWS-FLI1* and is countered by LIN28B in LIN28B$^+$ cells. Alternatively, the stability of EWS-FLI1 may be ensured at the protein level in LIN28B$^-$ EwS cells. Regardless of the mechanism, and unlike hpMSCs, LIN28B$^-$ EwS cells appear to have established, possibly over time, regulatory mechanisms of *EWS-FLI1* expression that are independent of and unresponsive to LIN28B.

A more fundamental question is why should LIN28B be indispensable for EWS-FLI1 expression in a subset of EwS? One possibility is that LIN28B provides the permissiveness required for EWS-FLI1-mediated transformation of the primary cells from which the LIN28B$^+$ EwS subclass originates. This notion would suggest that LIN28B$^+$ and LIN28B$^-$ EwS may have different cells of origin. In response to LIN28B expression, hpMSCs increase their proliferation, upregulate EWS-FLI1 target genes, and augment EWS-FLI1 expression. However, they do not require LIN28B expression for long-term EWS-FLI1 maintenance (Riggi et al., 2008). In most malignancies in which LIN28B expression becomes induced as a consequence of reprogramming linked to transformation, its expression is heterogeneous and is often confined to poorly differentiated cells that may display CSC features (Balzeau et al., 2017). In contrast, LIN28B$^+$ EwS express LIN28B in virtually all cells, suggesting that these tumors may arise from a stem or an early progenitor cell that has not turned off LIN28B expression. Interrogation of a published expression array of 33 normal adult tissues, which includes human neural crest stem cells (NCSCs) and MSCs (GEO accession: GSE68776), revealed high LIN28B expression in NCSCs and NC-derived MSCs (NC-MSCs) but low to undetectable expression in bone marrow MSCs (BM-MSCs) (Figure S4E). All 3 cell types are permissive for EWS-FLI1 expression (Riggi et al., 2005, 2008, 2010; von Levetzow et al., 2011), but their permissiveness may invoke different mechanisms. Thus, the expression of *EWS-FLI1* in NCSCs and NC-MSCs may require LIN28B and thereby lead to the development of LIN28B$^+$ EwS, whereas in BM-MSCs, it may result in LIN28B$^-$ tumors, which may rely on alternative mechanisms to ensure *EWS-FLI1* stability.

Treatment of EwS cells with the 1632 compound that blocks LIN28B binding to let-7 precursors and disrupts the LIN28B-mediated inhibition of let-7 maturation did not affect LIN28B$^-$ cell behavior, but it did abrogate LIN28B$^+$ cell self-renewal. Even limited pre-treatment of LIN28B$^+$ cells before injection into mice blunted their tumorigenicity, reflecting the extent of their dependence on LIN28B. Although these effects are consistent with increased let-7 expression, the 1632 inhibitor also caused a decrease in EWS-FLI1 and its target gene expression, which are let-7 independent. There are at least two non-mutually exclusive explanations for this seemingly counterintuitive observation. As LIN28B mRNA-binding sites have not been exhaustively elucidated (Mayr and Heinemann, 2013), it is possible that the inhibitor may interfere with LIN28B binding to *EWS-FLI1* transcripts, particularly in view of the discovery that some *LIN28B* mRNA consensus binding sites are similar to those of

Figure 7. The LIN28 Inhibitor 1632 Acts Selectively on LIN28B$^+$ EwS Cells, Leading to a Marked Reduction in Their Self-Renewal and Tumorigenic Properties

(A) Left panel: qRT-PCR analysis of mature let7-a, b, and f expression in EwS1 and EwS4 cells, treated with increasing concentrations of the 1632 inhibitor (50 and 250 μM), compared to that in the same cells treated with solvent alone (equivalent volume of DMSO, CTRL). Mean values ± SEMs of 3 independent experiments are shown. Right panel: qRT-PCR analysis of *HMGA2* expression in EwS1–EwS4 cultures treated with 250 μM of the 1632 inhibitor and assessed at days 0, 4, and 7 (means ± SEMs of 3 technical replicates). Two-way ANOVA was used for statistical analysis.

(B) Micrographs of EwS1 and EwS4 sphere cultures after 96 h of treatment with DMSO (CTRL) or 250 μM of the 1632 inhibitor.

(C) Clonogenic assay on EwS1–EwS4 cells treated with DMSO (CTRL) or 250 μM of the 1632 inhibitor (means ± SDs of 3 technical replicates).

(D) Venn diagram showing overlap among 4 gene datasets, including *LIN28B* knockdown, *EWS-FLI1* knockdown, and treatment with 250 μM of the 1632 inhibitor at 7 days (common downregulated genes); and the list of 99 direct EWS-FLI1 target genes described in Figure 5C.

(E) qRT-PCR assessment of *LIN28B*, *EWS-FLI1*, and WT *EWS* expression, as well as that of a panel of known direct EWS-FLI1 target genes in EwS1 cells following 7 days of treatment with the 1632 compound compared to that in the same cells treated with solvent alone for the same period of time. Mean values ± SEMs from 3 independent experiments are shown. Two-way ANOVA was used for statistical analysis.

(F) *In vivo* tumorigenicity assay after the injection of 1×10^4 EwS1 (left panel) or EwS2 (right panel) cells following 96 h of treatment with 250 μM of the 1632 inhibitor or solvent (equivalent volume of DMSO, CTRL). The bar indicates the mean value.

*p ≤ 0.05; ****p ≤ 0.0001; ns, non-significant. See also Figure S5.

let-7 precursors (Hafner et al., 2013; Wilbert et al., 2012). Alternatively, the depletion of *LIN28B* by increased let-7 maturation may result in the progressive loss of EWS-FLI1 expression and deconstruction of its target gene network. Although it may be relevant to a minority of patients, the exquisite dependence of EWS-FLI1 expression on LIN28B function may provide an unprecedented therapeutic perspective for EwS.

STAR★METHODS

Detailed methods are provided in the online version of this paper and include the following:

- KEY RESOURCES TABLE
- LEAD CONTACT AND MATERIALS AVAILABILITY
- EXPERIMENTAL MODEL AND SUBJECT DETAILS
  - Primary tumors and cell lines cultures
  - Animal Studies
- METHOD DETAILS
  - Plasmids and Lentiviral Infection
  - RNA *In Situ* Hybridization, Immunohistochemistry and Western Blot Analyses
  - RNA Isolation and Real-Time qPCR
  - Cell vitality, proliferation assays and drug tests
  - Nascent RNA capture and cDNA synthesis
  - *In vivo* tumorigenicity assays
  - RNA Immunoprecipitation
  - Achilles scores and survival analysis
  - LIN28B expression in an Ewing sarcoma dataset
  - Analysis of RNA-seq data
  - MicroRNA expression analysis
  - Overlap between differentially expressed genes and gene sets
- QUANTIFICATION AND STATISTICAL ANALYSIS
- DATA AND CODE AVAILABILITY

SUPPLEMENTAL INFORMATION

Supplemental Information can be found online at https://doi.org/10.1016/j.celrep.2019.12.053.

ACKNOWLEDGMENTS

This work was supported by Swiss National Science Foundation grants 310030_150024 and 310030_169563, Switzerland and Oncosuisse grant KLS-3365-02-2014, Switzerland (to I.S.); and a Swiss National Science Foundation grant PP00P3_157468, Switzerland, an Oncosuisse grant KFS-3973-08-2016, Switzerland, and a MEDIC Foundation grant, Switzerland (to N.R.). M.N.R. is supported by an award from the V Foundation, United States.

AUTHOR CONTRIBUTIONS

Conception & Design, N.R. and I.S.; Investigation & Methodology, M.T., G.B., S.C.-B., P.W., N.C., A.B., A.V., A.K., T.K., T.G., C.F., and P.M.; Data Analysis, M.N.R., P.P., N.R., S.I., and M.L.S.; Resources, I.L., S.C., G.M.C., E.C., A.D., M.M., I.C., P.G.N., A.M.C., J.M., R.R., and I.S.; Writing, Review, & Editing, G.B., N.R., M.N.R., and I.S.; Study Supervision, N.R. and I.S.; Funding Acquisition, I.S.

DECLARATION OF INTERESTS

The authors declare no competing interests.

Received: October 2, 2018
Revised: June 19, 2019
Accepted: December 13, 2019
Published: March 31, 2020; corrected online April 6, 2020

REFERENCES

Agarwal, V., Bell, G.W., Nam, J.W., and Bartel, D.P. (2015). Predicting effective microRNA target sites in mammalian mRNAs. eLife *4*, e05005.

Aguirre, A.J., Meyers, R.M., Weir, B.A., Vazquez, F., Zhang, C.Z., Ben-David, U., Cook, A., Ha, G., Harrington, W.F., Doshi, M.B., et al. (2016). Genomic Copy Number Dictates a Gene-Independent Cell Response to CRISPR/Cas9 Targeting. Cancer Discov. *6*, 914–929.

Aken, B.L., Achuthan, P., Akanni, W., Amode, M.R., Bernsdorff, F., Bhai, J., Billis, K., Carvalho-Silva, D., Cummins, C., Clapham, P., et al. (2017). Ensembl 2017. Nucleic Acids Res. *45* (*D1*), D635–D642.

Balzeau, J., Menezes, M.R., Cao, S., and Hagan, J.P. (2017). The LIN28/let-7 Pathway in Cancer. Front. Genet. *8*, 31.

Barretina, J., Caponigro, G., Stransky, N., Venkatesan, K., Margolin, A.A., Kim, S., Wilson, C.J., Lehár, J., Kryukov, G.V., Sonkin, D., et al. (2012). The Cancer Cell Line Encyclopedia enables predictive modelling of anticancer drug sensitivity. Nature *483*, 603–607.

Boulay, G., Sandoval, G.J., Riggi, N., Iyer, S., Buisson, R., Naigles, B., Awad, M.E., Rengarajan, S., Volorio, A., McBride, M.J., et al. (2017). Cancer-Specific Retargeting of BAF Complexes by a Prion-like Domain. Cell *171*, 163–178.e19.

Boulay, G., Volorio, A., Iyer, S., Broye, L.C., Stamenkovic, I., Riggi, N., and Rivera, M.N. (2018). Epigenome editing of microsatellite repeats defines tumor-specific enhancer functions and dependencies. Genes Dev. *32*, 1008–1019.

Brohl, A.S., Solomon, D.A., Chang, W., Wang, J., Song, Y., Sindiri, S., Patidar, R., Hurd, L., Chen, L., Shern, J.F., et al. (2014). The genomic landscape of the Ewing Sarcoma family of tumors reveals recurrent STAG2 mutation. PLoS Genet. *10*, e1004475.

Carmel-Gross, I., Bollag, N., Armon, L., and Urbach, A. (2016). LIN28: A Stem Cell Factor with a Key Role in Pediatric Tumor Formation. Stem Cells Dev. *25*, 367–377.

Carvalho, B.S., and Irizarry, R.A. (2010). A framework for oligonucleotide microarray preprocessing. Bioinformatics *26*, 2363–2367.

Chatterji, P., and Rustgi, A.K. (2018). RNA Binding Proteins in Intestinal Epithelial Biology and Colorectal Cancer. Trends Mol. Med. *24*, 490–506.

Chatterji, P., Hamilton, K.E., Liang, S., Andres, S.F., Wijeratne, H.R.S., Mizuno, R., Simon, L.A., Hicks, P.D., Foley, S.W., Pitarresi, J.R., et al. (2018). The LIN28B-IMP1 post-transcriptional regulon has opposing effects on oncogenic signaling in the intestine. Genes Dev. *32*, 1020–1034.

Choi, S.H., Kim, S.H., Shim, K.W., Han, J.W., Choi, J., Kim, D.S., Lyu, C.J., Kim, J.W., Suh, C.O., and Cho, J. (2016). Treatment Outcome and Prognostic Molecular Markers of Supratentorial Primitive Neuroectodermal Tumors. PLoS One *11*, e0153443.

Chuang, T.H., and Ulevitch, R.J. (2004). Triad3A, an E3 ubiquitin-protein ligase regulating Toll-like receptors. Nat. Immunol. *5*, 495–502.

Cornaz-Buros, S., Riggi, N., DeVito, C., Sarre, A., Letovanec, I., Provero, P., and Stamenkovic, I. (2014). Targeting cancer stem-like cells as an approach to defeating cellular heterogeneity in Ewing sarcoma. Cancer Res. *74*, 6610–6622.

Crompton, B.D., Stewart, C., Taylor-Weiner, A., Alexe, G., Kurek, K.C., Calicchio, M.L., Kiezun, A., Carter, S.L., Shukla, S.A., Mehta, S.S., et al. (2014). The genomic landscape of pediatric Ewing sarcoma. Cancer Discov. *4*, 1326–1341.

De Vito, C., Riggi, N., Suvà, M.L., Janiszewska, M., Horlbeck, J., Baumer, K., Provero, P., and Stamenkovic, I. (2011). Let-7a is a direct EWS-FLI-1 target implicated in Ewing's sarcoma development. PLoS One *6*, e23592.

De Vito, C., Riggi, N., Cornaz, S., Suvà, M.L., Baumer, K., Provero, P., and Stamenkovic, I. (2012). A TARBP2-dependent miRNA expression profile underlies cancer stem cell properties and provides candidate therapeutic reagents in Ewing sarcoma. Cancer Cell *21*, 807–821.

Dunker, A.K., and Uversky, V.N. (2010). Drugs for 'protein clouds': targeting intrinsically disordered transcription factors. Curr. Opin. Pharmacol. *10*, 782–788.

Engert, F., Schneider, C., Weiß, L.M., Probst, M., and Fulda, S. (2015). PARP Inhibitors Sensitize Ewing Sarcoma Cells to Temozolomide-Induced Apoptosis via the Mitochondrial Pathway. Mol. Cancer Ther. *14*, 2818–2830.

Erkizan, H.V., Kong, Y., Merchant, M., Schlottmann, S., Barber-Rotenberg, J.S., Yuan, L., Abaan, O.D., Chou, T.H., Dakshanamurthy, S., Brown, M.L., et al. (2009). A small molecule blocking oncogenic protein EWS-FLI1 interaction with RNA helicase A inhibits growth of Ewing's sarcoma. Nat. Med. *15*, 750–756.

Filbin, M.G., Tirosh, I., Hovestadt, V., Shaw, M.L., Escalante, L.E., Mathewson, N.D., Neftel, C., Frank, N., Pelton, K., Hebert, C.M., et al. (2018). Developmental and oncogenic programs in H3K27M gliomas dissected by single-cell RNA-seq. Science *360*, 331–335.

Hafner, M., Max, K.E., Bandaru, P., Morozov, P., Gerstberger, S., Brown, M., Molina, H., and Tuschl, T. (2013). Identification of mRNAs bound and regulated by human LIN28 proteins and molecular requirements for RNA recognition. RNA *19*, 613–626.

Hennchen, M., Stubbusch, J., Abarchan-El Makhfi, I., Kramer, M., Deller, T., Pierre-Eugene, C., Janoueix-Lerosey, I., Delattre, O., Ernsberger, U., Schulte, J.B., and Rohrer, H. (2015). Lin28B and Let-7 in the Control of Sympathetic Neurogenesis and Neuroblastoma Development. J. Neurosci. *35*, 16531–16544.

Javelaud, D., Wietzerbin, J., Delattre, O., and Besançon, F. (2000). Induction of p21Waf1/Cip1 by TNFalpha requires NF-kappaB activity and antagonizes apoptosis in Ewing tumor cells. Oncogene *19*, 61–68.

Jiang, J., Lee, E.J., Gusev, Y., and Schmittgen, T.D. (2005). Real-time expression profiling of microRNA precursors in human cancer cell lines. Nucleic Acids Res. *33*, 5394–5403.

Li, B., and Dewey, C.N. (2011). RSEM: accurate transcript quantification from RNA-Seq data with or without a reference genome. BMC Bioinformatics *12*, 323.

Madison, B.B., Liu, Q., Zhong, X., Hahn, C.M., Lin, N., Emmett, M.J., Stanger, B.Z., Lee, J.S., and Rustgi, A.K. (2013). LIN28B promotes growth and tumorigenesis of the intestinal epithelium via Let-7. Genes Dev. *27*, 2233–2245.

Madison, B.B., Jeganathan, A.N., Mizuno, R., Winslow, M.M., Castells, A., Cuatrecasas, M., and Rustgi, A.K. (2015). Let-7 Represses Carcinogenesis and a Stem Cell Phenotype in the Intestine via Regulation of Hmga2. PLoS Genet. *11*, e1005408.

Mayr, F., and Heinemann, U. (2013). Mechanisms of Lin28-mediated miRNA and mRNA regulation–a structural and functional perspective. Int. J. Mol. Sci. *14*, 16532–16553.

Nakhaei, P., Mesplede, T., Solis, M., Sun, Q., Zhao, T., Yang, L., Chuang, T.H., Ware, C.F., Lin, R., and Hiscott, J. (2009). The E3 ubiquitin ligase Triad3A negatively regulates the RIG-I/MAVS signaling pathway by targeting TRAF3 for degradation. PLoS Pathog. *5*, e1000650.

Picard, D., Miller, S., Hawkins, C.E., Bouffet, E., Rogers, H.A., Chan, T.S., Kim, S.K., Ra, Y.S., Fangusaro, J., Korshunov, A., et al. (2012). Markers of survival and metastatic potential in childhood CNS primitive neuro-ectodermal brain tumours: an integrative genomic analysis. Lancet Oncol. *13*, 838–848.

Pishas, K.I., and Lessnick, S.L. (2016). Recent advances in targeted therapy for Ewing sarcoma. F1000Res. *5*, F1000 Faculty Rev-2077.

Powers, J.T., Tsanov, K.M., Pearson, D.S., Roels, F., Spina, C.S., Ebright, R., Seligson, M., de Soysa, Y., Cahan, P., Theißen, J., et al. (2016). Multiple mechanisms disrupt the let-7 microRNA family in neuroblastoma. Nature *535*, 246–251.

R Development Core Team (2019). R: A language and environment for statistical computing (R Foundation for Statistical Computing).

Riggi, N., and Stamenkovic, I. (2007). The biology of Ewing sarcoma. Cancer Lett. *254*, 1–10.

Riggi, N., Cironi, L., Provero, P., Suvà, M.L., Kaloulis, K., Garcia-Echeverria, C., Hoffmann, F., Trumpp, A., and Stamenkovic, I. (2005). Development of Ewing's sarcoma from primary bone marrow-derived mesenchymal progenitor cells. Cancer Res. *65*, 11459–11468.

Riggi, N., Suvà, M.L., Suvà, D., Cironi, L., Provero, P., Tercier, S., Joseph, J.M., Stehle, J.C., Baumer, K., Kindler, V., and Stamenkovic, I. (2008). EWS-FLI-1 expression triggers a Ewing's sarcoma initiation program in primary human mesenchymal stem cells. Cancer Res. *68*, 2176–2185.

Riggi, N., Suvà, M.L., De Vito, C., Provero, P., Stehle, J.C., Baumer, K., Cironi, L., Janiszewska, M., Petricevic, T., Suvà, D., et al. (2010). EWS-FLI-1 modulates miRNA145 and SOX2 expression to initiate mesenchymal stem cell reprogramming toward Ewing sarcoma cancer stem cells. Genes Dev. *24*, 916–932.

Riggi, N., Knoechel, B., Gillespie, S.M., Rheinbay, E., Boulay, G., Suvà, M.L., Rossetti, N.E., Boonseng, W.E., Oksuz, O., Cook, E.B., et al. (2014). EWS-FLI1 utilizes divergent chromatin remodeling mechanisms to directly activate or repress enhancer elements in Ewing sarcoma. Cancer Cell *26*, 668–681.

Ritchie, M.E., Phipson, B., Wu, D., Hu, Y., Law, C.W., Shi, W., and Smyth, G.K. (2015). limma powers differential expression analyses for RNA-sequencing and microarray studies. Nucleic Acids Res. *43*, e47.

Roos, M., Pradère, U., Ngondo, R.P., Behera, A., Allegrini, S., Civenni, G., Zagalak, J.A., Marchand, J.R., Menzi, M., Towbin, H., et al. (2016). A Small-Molecule Inhibitor of Lin28. ACS Chem. Biol. *11*, 2773–2781.

Savola, S., Klami, A., Myllykangas, S., Manara, C., Scotlandi, K., Picci, P., Knuutila, S., and Vakkila, J. (2011). High Expression of Complement Component 5 (C5) at Tumor Site Associates with Superior Survival in Ewing's Sarcoma Family of Tumour Patients. ISRN Oncol. *2011*, 168712.

Shinoda, G., Shyh-Chang, N., Soysa, T.Y., Zhu, H., Seligson, M.T., Shah, S.P., Abo-Sido, N., Yabuuchi, A., Hagan, J.P., Gregory, R.I., et al. (2013). Fetal deficiency of lin28 programs life-long aberrations in growth and glucose metabolism. Stem Cells *31*, 1563–1573.

Suvà, M.L., Riggi, N., Stehle, J.C., Baumer, K., Tercier, S., Joseph, J.M., Suvà, D., Clément, V., Provero, P., Cironi, L., et al. (2009). Identification of cancer stem cells in Ewing's sarcoma. Cancer Res. *69*, 1776–1781.

Thornton, J.E., and Gregory, R.I. (2012). How does Lin28 let-7 control development and disease? Trends Cell Biol. *22*, 474–482.

Tirode, F., Laud-Duval, K., Prieur, A., Delorme, B., Charbord, P., and Delattre, O. (2007). Mesenchymal stem cell features of Ewing tumors. Cancer Cell *11*, 421–429.

Tirode, F., Surdez, D., Ma, X., Parker, M., Le Deley, M.C., Bahrami, A., Zhang, Z., Lapouble, E., Grossetête-Lalami, S., Rusch, M., et al.; St. Jude Children's Research Hospital–Washington University Pediatric Cancer Genome Project and the International Cancer Genome Consortium (2014). Genomic landscape of Ewing sarcoma defines an aggressive subtype with co-association of STAG2 and TP53 mutations. Cancer Discov. *4*, 1342–1353.

Tomazou, E.M., Sheffield, N.C., Schmidl, C., Schuster, M., Schönegger, A., Datlinger, P., Kubicek, S., Bock, C., and Kovar, H. (2015). Epigenome mapping reveals distinct modes of gene regulation and widespread enhancer reprogramming by the oncogenic fusion protein EWS-FLI1. Cell Rep. *10*, 1082–1095.

Urbach, A., Yermalovich, A., Zhang, J., Spina, C.S., Zhu, H., Perez-Atayde, A.R., Shukrun, R., Charlton, J., Sebire, N., Mifsud, W., et al. (2014). Lin28 sustains early renal progenitors and induces Wilms tumor. Genes Dev. *28*, 971–982.

Viswanathan, S.R., and Daley, G.Q. (2010). Lin28: a microRNA regulator with a macro role. Cell *140*, 445–449.

Viswanathan, S.R., Powers, J.T., Einhorn, W., Hoshida, Y., Ng, T.L., Toffanin, S., O'Sullivan, M., Lu, J., Phillips, L.A., Lockhart, V.L., et al. (2009). Lin28 promotes transformation and is associated with advanced human malignancies. Nat. Genet. *41*, 843–848.

von Levetzow, C., Jiang, X., Gwye, Y., von Levetzow, G., Hung, L., Cooper, A., Hsu, J.H., and Lawlor, E.R. (2011). Modeling initiation of Ewing sarcoma in human neural crest cells. PLoS One *6*, e19305.

Vormoor, B., and Curtin, N.J. (2014). Poly(ADP-ribose) polymerase inhibitors in Ewing sarcoma. Curr. Opin. Oncol. *26*, 428–433.

Wilbert, M.L., Huelga, S.C., Kapeli, K., Stark, T.J., Liang, T.Y., Chen, S.X., Yan, B.Y., Nathanson, J.L., Hutt, K.R., Lovci, M.T., et al. (2012). LIN28 binds messenger RNAs at GGAGA motifs and regulates splicing factor abundance. Mol. Cell *48*, 195–206.

Zhang, J., Ratanasirintrawoot, S., Chandrasekaran, S., Wu, Z., Ficarro, S.B., Yu, C., Ross, C.A., Cacchiarelli, D., Xia, Q., Seligson, M., et al. (2016). LIN28 Regulates Stem Cell Metabolism and Conversion to Primed Pluripotency. Cell Stem Cell *19*, 66–80.

STAR★METHODS

KEY RESOURCES TABLE

REAGENT or RESOURCE	SOURCE	IDENTIFIER
Antibodies		
Rabbit polyclonal anti-EWS	Bethyl	Cat#A300-418A; RRID: AB_420958
Mouse monoclonal anti-Tubulin	Millipore	Cat#CP06; RRID: AB_2617116
Rabbit polyclonal anti-FLI1	Abcam	Cat#ab15289; RRID: AB_301825
Rabbit Anti-Human LIN28B Polyclonal Antibody	Proteintech	Cat# 16178-1-AP; RRID:AB_2135051
Rabbit Anti-Human LIN28B Polyclonal Antibody	Cell Signaling Technology	Cat# 4196; RRID:AB_2135047
Monoclonal Anti-GAPDH-Peroxidase antibody produced in mouse	Sigma-Aldrich	Cat# G9295; RRID:AB_1078992
Anti-Rabbit IgG (whole molecule)-Peroxidase antibody produced in goat	Sigma-Aldrich	Cat#A0545; RRID:AB_257896
Biological Samples		
EwS1-4	This paper	See Table S3
hpMSC1-2	This paper	See Method Details
Chemicals, Peptides, and Recombinant Proteins		
IMDM, GlutaMAX SupplementIMDM	Thermofisher Scientific	Cat#31980022
DMEM, high glucose, GlutaMAX Supplement, pyruvate	Thermofisher Scientific	Cat#31966021
KnockOut Serum Replacement - Multi-Species	Thermofisher Scientific	Cat#10828028
FBS Good Forte	PAN BIOTECH	Cat#P40-49500
Trypsin-EDTA (0.05%), phenol red	Thermofisher Scientific	Cat#25300062
MEM Non-Essential Amino Acids Solution	Thermofisher Scientific	Cat#11140035
Penicillin-Streptomycin (10,000 U/mL)	Thermofisher Scientific	Cat#15140122
EGF Human	PROSPEC Protein specialists	Cat#CYT-217
FGF 2 Human	PROSPEC Protein specialists	Cat#CYT-218
Fugene 6	Promega	Cat#E2692
Polybrene	Sigma-Aldrich	Cat#005557
Puromycin	InvivoGen	Cat#ant-pr-1
PowerUp SYBR Green Master Mix	Applied Biosystems	Cat#A25742
Calcein AM cell-permeable-dye	Life Technologies	Cat#C1430
Lin28 1632	Tocris Bioscience	Cat#6068
Dimethyl sulfoxide	Sigma-Aldrich	Cat#41640
Actinomycin D	Sigma-Aldrich	Cat#A1410
VectaMount® AQ Aqueous Mounting Medium	Vector Laboratories	Cat#H-5501
M-MLV Reverse Transcriptase	Promega	Cat#M170B
RNasin Ribonuclease inhibitor	Promega	Cat#N211B
RPMI 1640 Medium, GlutaMAX Supplement	Thermofisher Scientific	Cat#61870010
Lin28B RNAscope® Probe	ACD	Cat#596361
dNTP set	MP Biomedicals	Cat#11NTACG100-CF
Doxycycline hyclate	Sigma-Aldrich	Cat#D9891
Geneticin	Thermofisher Scientific	Cat#10131-027
FBS (tetracyclin-free)	PAN BIOTECH	Cat#P30-3602
Ketasol-100	Dr. E. Graeub AG	Cat#668.51
Rompun 2%	Provet AG	Cat#1315

(*Continued on next page*)

Continued

REAGENT or RESOURCE	SOURCE	IDENTIFIER
PDGF-BB	PeproTech	Cat#100-14B
Critical Commercial Assays		
miRCURY RNA Isolation Kit - Cell & Plant	Exiqon	Cat#300110
Click-iT Nascent RNA Capture Kit	Life Technologies	Cat#10365
NucleoSpin miRNA kit	Macherey-Nagel	Cat#740971
EZ-Magna RIP™ RNA-Binding Protein Immunoprecipitation kit	MerckMillipore	Cat#PP64B
CellTiter 96® AQ_{ueous} One Solution Cell Proliferation Assay	Promega	Cat#G3582
Deposited Data		
Gene expression data for Ewing sarcoma spheres generated for this project	This Paper	GEO: GSE122632
Gene expression data for primary Ewing sarcomas	Savola et al., 2011	GEO: GSE17618
Gene expression data for primary Ewing sarcomas	Brohl et al., 2014	https://pob.abcc.ncifcrf.gov/cgi-bin/JK
Gene sets for functional enrichment analysis	Broad Institute	Molecular Signatures Database, RRID:SCR_016863
ATARIS gene scores	Aguirre et al., 2016	https://depmap.org/portal/download/
Experimental Models: Cell Lines		
Lenti-X 293T	Clontech	Cat#632180
A-673	ATCC	Cat# CRL-1598, RRID:CVCL_0080
Experimental Models: Organisms/Strains		
NNOD.Cg-Prkdc^{scid} Il2rg^{tm1Wjl}/SzJ	The Jackson Laboratory	RRID:IMSR_JAX:005557
Oligonucleotides		
Random Primers	Promega	Cat#C118A
Primer sequences for real-time PCR	This paper	see Table S5
sgRNA targeting Lin28B (exon2): CACCGCATCGACTGGAATATCCAAG	Powers et al., 2016	N/A
Recombinant DNA		
shRNA Lin28B n.1	Broad Institute, RNAi Consortium	Cat#TRCN0000219859
shRNA Lin28B n.2	Broad Institute, RNAi Consortium	Cat#TRCN0000122191
shRNA targeting EWS-FLI-1	Tirode et al., 2007	N/A
pInd EWS-FLI1	Boulay et al., 2017	N/A
Software and Algorithms		
FlowJo version 9.9.4	FLOWJI, LLC	https://www.flowjo.com/solutions/flowjo/, RRID:SCR_008520
Adobe Illustrator CC 2015	Adobe	https://www.adobe.com/products/illustrator.html, RRID:SCR_010279
GraphPad Prism version 8	GraphPad Software	https://www.graphpad.com/, RRID:SCR_002798
Oligo	Carvalho and Irizarry, 2010	Bioconductor, RRID:SCR_006442
Limma	Ritchie et al., 2015	Bioconductor, RRID:SCR_006442
R Project for Statistical Computing	R Development Core Team, 2019	R Project for Statistical Computing, RRID:SCR_001905
RSEM	Li and Dewey, 2011	https://github.com/deweylab/RSEM
Other		
Ensembl	Aken et al., 2017	Ensembl Genome Browser, RRID:SCR_013367
TargetScan	Agarwal et al., 2015	TargetScan, RRID:SCR_010845

LEAD CONTACT AND MATERIALS AVAILABILITY

Further information and requests for resources and reagents should be directed to and will be fulfilled by the Lead Contact, Ivan Stamenkovic (Ivan.Stamenkovic@chuv.ch). All unique/stable reagents generated in this study are available from the Lead Contact with a completed Materials Transfer Agreement.

EXPERIMENTAL MODEL AND SUBJECT DETAILS

Primary tumors and cell lines cultures

Primary EwS and MSC samples from the University Hospital of Lausanne (CHUV) were obtained at surgery with the approval of the Ethics Committee of the Canton de Vaud (project authorization No. 131/12). For samples received from the Hospital Sant Joan de Déu (HSJD, Barcelona), written informed consent was obtained from all patients prior to inclusion of their samples in the tumor biobank, following procedures approved by the Ethical Committee for Clinical Research at HSJD (M. 1608-C). All human samples were anonymized before analysis and were exempted from informed consent in accordance with the law of the Canton de Vaud. Table S3 lists LIN28B status, age, sex, tumor site, tumor staging, treatment status, EwS-FLI1 translocation details of EwS1-4 samples. Primary EwS spheres were cultured in IMDM (GIBCO), supplemented with 20% KO serum (GIBCO), 10ng/mL human recombinant EGF and bFGF (PROSPEC), and 1% Pen/Strep (GIBCO) in ultra-low attachment flasks (Corning), as previously described (Suvà et al., 2009).

HpMSCs were obtained from bone marrow of two healthy pediatric patients undergoing corrective surgery as described previously (Riggi et al., 2008). Both HpMSC1 and HhMSC2 were obtained from male patients. HpMSCs were cultured at low confluence in IMDM (GIBCO), 10% FCS (PAN BIOTECH), 10ng/mL PDGF-BB (PeproTech), and 1% Pen/Strep (GIBCO), and were tested for multilineage differentiation into adipocytes, chondrocytes, and osteoblasts (Riggi et al., 2008).

The Lenti-X 293T cell line was purchased from Clontech (cat no. 632180) and grown in DMEM medium (GIBCO) supplemented with 10% FCS (PAN BIOTECH) and 1% Pen/Strep (GIBCO). The A673 cell line was purchased from ATCC (cat no. CRL-1598) and grown in RPMI (GIBCO) supplemented with 10% FCS (PAN BIOTECH) and 1% Pen/Strep (GIBCO).

Cell cultures were maintained at 37°C and 5% CO_2 in humidified culture incubators.

Animal Studies

Experimental protocols involving mice were approved by the Veterinary Service of the Canton of Vaud, Switzerland (Etat de Vaud, Service Vétérinaire) under the authorization number VD2488. NOD-*scid* IL2Rgamma^{null} mice (NSG) purchased from The Jackson Laboratory, USA (stock number 005557) were used in this study. All mice were 6-8 weeks old males. Mice were maintained in a pathogen-free environment in individual ventilated cages and fed with autoclaved food and water at the animal Facility of the University of Lausanne.

METHOD DETAILS

Plasmids and Lentiviral Infection

Stable LIN28B depletion was obtained using either pLKO.1 lentiviral shRNA vectors purchased from the RNAi Consortium (shRNA n.1 ref. TRCN0000219859; shRNA n.2 ref. TRCN0000122191), or a previously described sgRNA targeting LIN28B exon 2 (Powers et al., 2016) cloned into the lentiCRISPRv2 vector. Control cells were infected with shRNA and sgRNA sequences targeting the *GFP* transcripts (GCAAGCTGACCCTGAAGTTCAT). The shRNA sequence used for EWS-FLI1 depletion was previously described and validated (Tirode et al., 2007). For LIN28B overexpression, the *LIN28B* cDNA was amplified from A673 cells and cloned into the pLIV lentiviral vector. Lentiviruses were produced using Lenti-X 293T packaging cells, transfected with the plasmid of interest, GAG/POL and VSV using FuGene 6 (Promega). In all cases, EwS cell suspensions from dissociated spheres were subject to lentiviral infection for 8hrs in the presence of 6μg/mL Polybrene (Sigma-Aldrich), and cells were selected with 1μg/mL puromycin (InvivoGen) for 48hrs prior to further analysis, as previously described (De Vito et al., 2012). HpMSCs infected with the pInd EWS-FLI1 V5 lentiviral vector (Boulay et al., 2017) were selected with 1500μg/mL geneticin (ThermoFisher Scientific) for 8 days and then treated with 1 μg/mL doxycycline (Sigma-Aldrich) for 8 supplementary days with medium renewal every other day.

RNA *In Situ* Hybridization, Immunohistochemistry and Western Blot Analyses

RNAscope technology (Advanced Cell Diagnostics, ACD) was used for RNA *in situ* hybridization following the manufacturer's instructions as described previously (Filbin et al., 2018). Briefly, slides were baked for 1hr at 60°C, deparaffinized and dehydrated. The tissue was pretreated with Hydrogen Peroxide for 10 minutes at room temperature and with Target Retrieval Reagent for 15 minutes at 98°C. Protease Plus was then applied for 30 minutes at 40°C. LIN28B probe (ACD) was hybridized for 2hrs at 40°C, followed by signal amplification. Tissue was counterstained with Gill's hematoxylin followed by mounting with VectaMount mounting media (Vector Laboratories).

For immunohistochemistry (IHC) EwS spheres were re-suspended in 1.5% low-melting agarose and included in paraffin blocks. The blocks were sectioned and stained using LIN28B-specific polyclonal antibody (Proteintech). The signal was revealed using goat anti-rabbit Ig conjugated to HRP (Sigma-Aldrich).

Western blots were analyzed according to standard procedures. The antibodies used were: rabbit polyclonal anti-human LIN28B antibody (Cell Signaling Technology), mouse monoclonal anti-GAPDH peroxidase conjugated antibody (Sigma-Aldrich), mouse monoclonal anti-α-tubulin antibody (Millipore), rabbit polyclonal anti-FLI1 antibody (Abcam), rabbit polyclonal anti-EWS antibody (Bethyl Laboratories).

RNA Isolation and Real-Time qPCR

Total RNA was isolated using miRCURY RNA Isolation Kit – Cell & Plant (Exiqon) according to the manufacturer's recommendations. Real-time qPCR was performed as previously described (Riggi et al., 2010) using PowerUp SYBR Green (Applied Biosystems). Primer sequences used for gene expression are listed in Table S5. Relative gene expression levels were calculated with the DDCt method after normalization of the Ct values to the geometric mean of the Ct values of three housekeeping genes (*GAPDH*, *36B4* and *TBP*). SYBR Green primers for miRNA immature forms were previously published (Jiang et al., 2005). For miRNA mature form expression quantification, RT-qPCR was performed as previously described (Cornaz-Buros et al., 2014).

Cell vitality, proliferation assays and drug tests

For cell viability assays, freshly dissociated spheres were stained with 1μg/mL Calcein AM cell-permeable-dye (ThermoFisher Scientific) and analyzed by FACS. For clonogenic assays Calcein-positive single cells were FACS-sorted onto ultra-low attachment 96-well plates (Corning) and cultured in complete KO medium for 15 days, when sphere formation was assessed. Cell proliferation was determined by MTS assays (CellTiter 96, Promega), according to the manufacturer's recommendations.

For pharmacological targeting of LIN28B, the 1632 chemical inhibitor (Tocris) was dissolved in DMSO (Sigma-Aldrich) according to the manufacturer's recommendations. EwS spheres were dissociated and re-suspended in 6-well plates (Corning) in complete medium containing either solvent (DMSO) or the 1632 inhibitor at day 0. The drug was added at a concentration of 50 or 250μM, and an equal volume of DMSO without the drug was used as a control. Media were aspirated on day 4 and replaced with fresh medium containing DMSO or the inhibitor.

For clonogenic assays, spheres were pre-treated with DMSO or the 1632 inhibitor for 4 days, then resuspended, stained with 1μg/mL Calcein AM cell-permeable-dye (ThermoFisher Scientific) and single Calcein-positive cells were FACS-sorted onto ultra-low attachment 96-well plates (Corning) containing medium with DMSO or the 1632 inhibitor. Media were removed on day 7 and replaced with fresh medium containing DMSO or the inhibitor. For *in vivo* tumorigenicity assays, EwS spheres were pre-treated in culture for 4 days with DMSO or the inhibitor prior to injection.

For the analysis of *EWS-FLI1* RNA stability, EwS2 cells were treated with 10μg/mL of ActD (Sigma-Aldrich), or an equal volume of solvent (DMSO) as control. Cells were infected with shCTRL or sh2 LIN28B lentiviral vectors. ActD or DMSO were added 36hrs later, and RNA was harvested at 0, 4, 8, 12 and 24hrs post-ActD treatment. Relative gene expression levels were calculated by real-time qPCR using DDCt method normalized to *GAPDH* expression levels.

Nascent RNA capture and cDNA synthesis

Nascent RNA capture was performed with a Click-iT Nascent RNA Capture Kit (Life Technologies) according to the manufacturer's instructions. Briefly, cells were incubated with 5-EU at a concentration of 0.5mM for 30 minutes. Total RNA was isolated using NucleoSpin miRNA kit (Macherey-Nagel) and biotinylated. Following RNA precipitation, Dynabeads provided in the kit were used to isolate the nascent RNA with incorporated 5-EU. For cDNA synthesis from the bound nascent RNA, the bead suspension was warmed at 70°C for 5 minutes. Random primers (Promega) and dNTP (MP Biomedicals) were immediately added to the mixture. The suspension was left to cool down to room temperature for 30 minutes under constant rotation. M-MLV Reverse Transcriptase (Promega) and RNasin Ribonuclease inhibitor (Promega) were subsequently added to the suspension, which was then warmed to 42°C for 1hr with gentle vortexing. Finally, the cDNA was collected after heating the solution for 5 minutes at 85°C.

In vivo tumorigenicity assays

For kidney subcapsular injections mice were anesthetized using 100mg/kg Ketamine (Ketasol-100, Graueb AG) and 16mg/kg Xylazine (Rompun 2%, Provet AG) dissolved in PBS and $1x10^4$ sphere-derived cells were injected beneath the renal capsule. Tumor growth was monitored weekly using ultrasound imaging (Vevo 2100 Ultrasound Device, 40-MHz probe, VisualSonics, Canada). Tumor volume was calculated by the following formula: $V = 4/3\ \pi \times (Dd \times Ds \times Dt)/8$, where D*d* corresponds to tumor height, and D*s* and D*t* to tumor lengths measured in long- and short-axis views, respectively. For the experiment in Figure 2, mice were sacrificed when tumors reached $1cm^3$. For the experiments in Figures 3 and 6, mice were sacrificed when control tumors reached $1cm^3$. For the experiment in Figure 5, mice where sacrificed 8 weeks after injection. Harvested tumors were further processed for RNA extraction, hematoxylin/eosin staining, and IHC.

RNA Immunoprecipitation

RNA immunoprecipitation (RIP) on total EwS1 and EwS2 cell lysates was conducted using the EZ-Magna RIP™ RNA-Binding Protein Immunoprecipitation kit (MerckMillipore), according to the manufacturer's instructions. Rabbit polyclonal anti-human LIN28B antibody (Cell Signaling Technology) was diluted 1:50, as recommended by the manufacturer. Briefly, following gentle lysis of the cells at −80°C, total lysates were incubated overnight with anti-LIN28B antibody pre-bound to magnetic beads provided with the kit. The

beads were then rinsed and the antibody-protein-RNA complexes were dissociated by proteinase K digestion for 30 minutes. RNA was purified using the miRCURY RNA Isolation Kit - Cell & Plant (Exiqon) and enrichment of the selected LIN28B-bound transcripts was assessed by RT-qPCR. Ct values obtained for the genes of interest were normalized to Ct values obtained from 10% of the input (corresponding to the non-immunoprecipitated RNA obtained from the same sample).

Achilles scores and survival analysis

ATARIS scores were obtained from the project Achilles CRISPR screening data (Aguirre et al., 2016). The median ATARIS score for each gene was used to select the top 100 genes associated with the strongest reduction in EwS cells growth. To determine the correlation between the expression of these genes and survival in Ewing sarcoma we used the results of (Savola et al., 2011), available as GSE17618. Cox univariate analysis in the R computing environment (R Development Core Team, 2019, https://www.R-project.org) was used to determine the correlation between the expression of each gene and event-free survival.

LIN28B expression in an Ewing sarcoma dataset

We retrieved the gene-level normalized data of 65 primary Ewing tumors (Brohl et al., 2014) from Oncogenomicsdb and represented expression as log2(RPKM+1). Microarray data were retrieved as normalized expression levels from the respective GEO records (GSE17618; GSE34620; GSE12102). As the detection threshold, we used the median expression over all genes and samples. Correlation between gene expression and survival was evaluated by Cox univariate analysis on logarithmic expression values using event-free survival times. To assess possible associations between LIN28B status and somatic mutations in known oncogenes, we used Fisher exact test to determine whether tumors expressing LIN28B were significantly overrepresented among those carrying somatic mutations in *STAG2*, *CKDN2A*, *TP53*, or *BRCA2*, as reported in Table S5 of Brohl et al. (2014).

Analysis of RNA-seq data

Gene-level counts were obtained by aligning reads to the human transcriptome (Ensembl version 79 (Aken et al., 2017)) using RSEM (Li and Dewey, 2011). When comparing LIN28B-positive versus negative spheres we considered as differentially expressed the genes with absolute log2 fold-change greater than one in all four possible comparisons. For the shRNA and 1632 compound experiments, we considered as differentially expressed between two conditions the genes with log2(TPM+1) greater than 3 in at least one of the conditions and absolute log2 fold-change between the two conditions greater than one. The condition log2(TPM+1) in at least one of our samples was also used to select the genes used in analyzing the overlap between our differentially expressed genes and gene lists derived from external databases.

MicroRNA expression analysis

We used the Affymetrix miRNA 4.0 platform to compare miRNA expression between two LIN28B^{+} and two LIN28B^{-} tumors. RMA normalization and background subtraction were performed using the ''oligo'' Bioconductor package (Carvalho and Irizarry, 2010). Differential expression was evaluated using the ''limma'' Bioconductor package (Ritchie et al., 2015) and miRNAs with absolute log2 of fold change greater than 1 and nominal $p < 0.01$ were considered differentially expressed. Their expression z-score are shown in the heatmap of Figure 5A, together with the p value of the enrichment of their targets among genes that were found differentially expressed in LIN28B-positive versus negative spheres. Specifically, we evaluated, by exact Fisher test, the overlap between predicted targets of up- (down-) regulated miRNAs (obtained from TargetScan [Agarwal et al., 2015] and genes that are down- (up-) regulated in LIN28B^{+} spheres. The size of the overlap and the corresponding p values are shown beside the heatmap.

Overlap between differentially expressed genes and gene sets

The overlap between lists of differentially expressed genes and gene sets shown in the Venn diagrams was evaluated for statistical significance using exact Fisher test. The ''chemical and genetic perturbations'' gene sets of the Broad Institute MSIGDB database were obtained from their website. The heatmaps represent the expression z-score of the common genes in the conditions indicated.

QUANTIFICATION AND STATISTICAL ANALYSIS

Statistical analysis of wet lab experiments (Student's t test, 2-way ANOVA, Kaplan-Meyer test, Fisher's exact test) were performed by Prism GraphPad Software 8.00. All statistical tests and sample numbers are disclosed in respective Figure Legends/Supplementary Tables.

Statistical analysis of bioinformatics data are described in details in the ''Method Details'' section.

DATA AND CODE AVAILABILITY

Gene expression data generated for this project are available for the Gene Expression Omnibus repository under accession GSE122632 (https://www.ncbi.nlm.nih.gov/geo/query/acc.cgi?acc=GSE122632). All the software used in the analysis and the data generated for other publications are publicly available as detailed in the Key Resources Table.